Characterization of Hit Compounds that Inhibit Glucocorticoid Receptor Translocation in a Cell-Based High Content Screen

by

Timothy Ray Pouland

B.S. Biochemistry, University of Missouri, 2005

Submitted to the Graduate Faculty of

The School of Pharmacy in partial fulfillment

of the requirements for the degree of

Master of Science

University of Pittsburgh

2015

UNIVERSITY OF PITTSBURGH

School of Pharmacy

This Thesis was presented

by

Timothy Pouland

It was defended on

[OCTOBER 30, 2015]

and approved by

Dr. Jeffrey Brodsky, Professor, Avinoff Chair, Biological Science

Dr. Barry Gold, Professor, Chair, Pharmaceutical Sciences

Dr. Paul Johnston, Research Associate Professor, Pharmaceutical Sciences

Dr. Lisa Rohan, Associate Professor, Pharmaceutical Sciences

Dr. Wen Xie, Professor, Joseph Kaslow Endowed Chair, Pharmaceutical Sciences

Thesis Advisor: Dr. Maggie Folan, Assistant Professor, Pharmacy and Therapeutics

Characterization of Hit Compounds that Inhibit Glucocorticoid Receptor Translocation in a Cell-Based High Content Screen

Timothy Ray Pouland

University of Pittsburgh, 2015

The goal of these studies was to characterize hit compounds identified in a high-content screen of over 220,000 compounds in a glucocorticoid receptor (GR) translocation assay. Hit compounds were those compounds that reproducibly inhibited the dexamethasone-induced translocation of GR from the cytoplasm to the nucleus in a concentration dependent manner. The translocation of GR occurs after glucocorticosteroid binds the ligand binding domain of GR maintained in a high affinity binding state by ATP bound hsp90 in a hetero-complex that includes hsp70, hsp40, Hop, and p23.. After glucocorticosteroid is bound to GR, the GR attaches to cytoplasmic dynein and is transported from the cytoplasm to the nucleus. Because the translocation of GR from the cytoplasm to the nucleus depends on the activity of both hsp90 and cytoplasmic dynein it is possible that a sub-set of hit compounds from the HCS might be hsp90 or cytoplasmic dynein inhibitors. The focus of this study was shifted to identifying hsp90 inhibitors after failure to show proof of concept that the previously published cytoplasmic dynein inhibitors ciliobrevin A and D could inhibit GR translocation in the GR translocation assay. After verification that hsp90 inhibitors do inhibit GR translocation in the GR translocation assay, the hit compound list was reduced from approximately 112 compounds down to five compounds that were presumed likely to bind hsp90 based on computational analyses. An ATPase activity assay was developed to test these five hit compounds against hsp90 and two other ATPases,

myosin and kinesin; both of which are cytoskeletal motor proteins. Once these enzymes are optimized in the ATPase assay, they can be tested with the selected hit compounds.

TABLE OF CONTENTS

1.0 INTRODUCTION AND BACKGROUND……..1

1.1 INTRODUCTION……..…….1

1.2 HSP90…….……..10

1.3 HSP90 AS A DRUG TARGET……..…13

2.0 GR-GFP TRANSLOCATION ASSAY…….....14

2.1 INTRODUCTION…….14

2.2 SPECIFIC AIM…….15

2.3 METHODS……....15

2.4 RESULTS……..17

2.5 DISCUSSION…….30

3.0 SELECTION OF HIT COMPOUNDS TO FURTHER CHARACTERIZE……..32

3.1 INTRODUCTION…….32

3.2 SPECIFIC AIM……34

3.3 METHODS……34

3.4 RESULTS……..36

3.5 DISCUSSION……48

4.0 ATPASE ACTIVITY ASSAYS……..51

4.1 INTRODUCTION……51

4.2 SPECIFIC AIM……52

4.3 METHODS……52

4.4 RESULTS……..56

4.5 DISCUSSION……69

5.0 FURTHER DIRECTION……..70

REFERENCES..... 71

LIST OF TABLES

Table 1: PubChem Cross Target Query Results……..38

Table 2: Results of Instant Jchem Med Chem Analysis ……..…45

Table 3: Docking Scores from SYBYL Docking Simulation…...……...47

Table 4: Summary of 5 Hit Compounds Selected……50

LIST OF FIGURES

Figure 1: GR Ligand-binding Domain (cleft) Opening by Hsp70 and Hsp90……..5

Figure 2. The GR-hsp90-immunophilin Complex Attaches to Cytoplasmic Dynein for Retrograde Transport Along Microtubules Towards the Nucleus……...7

Figure 3. Structure of Hsp90……...……12

Figure 4. Color Composite Images of Dexamethasone Treated (B) and Untreated (A) 3617.4 Cells……...19

Figure 5. Determine Order of Aspiration and Fixation for Dexamethasone-induced GR-GFP Nuclear Translation…….....20

Figure 6. Time course of Dexamethasone-induced GR-GFP Nuclear Transport……21

Figure 7. GR-GFP Nuclear Translocation Dexamethasone Induced Concentration Response……..…….22

Figure 8. Inner/Outer Ratio and Average Outer and Inner Intensity of GFP in 3617.4 Cells Treated with Cytoplasmic Dynein Inhibitors……25

Figure 9. Average Outer and Inner Intensity of GFP Channel of 3617.4 Cells Treated With Cytoplasmic Dynein Inhibitors With No GFP……..26

Figure 10. 3617.4 Cells Treated With Microtubule Perturbagens, Hsp90, and Hsp70 Inhibitors…….…….29

Figure 11. ATP and Geldanamycin Binding Hsp90…… 36

Figure 12. Structures of Selected Hit Compounds……50

Figure 13. SDS-PAGE of Elution Fractions from Hsp90 Purification……..…….57

Figure 14. Enzyme Titration of Recombinant Yeast Hsp90……...58

Figure 15. Substrate Titration of Recombinant Yeast Hsp90…….....59

Figure 16. Hsp90 Prep Treated With 17-AAG…….……61

Figure 17. Enzyme Titration Kinesin Heavy Chain Motor Domain…….62

Figure 18. SubstrateTitration Kinesin HeavyChain Motor Domain…….64

Figure 19. Kinesin Treated With AMP-PNP…….……...……65

Figure 20. Myosin Enzyme Titration Testing Reaction Buffers…….66

Figure 21. Myosin Enzyme Titration in PiPerAssay……...67

Figure 22. Myosin Substrate Titration……..……68

1.0 INTRODUCTION AND BACKGROUND

1.1. INTRODUCTION

According to the American Cancer Society, approximately one of every four deaths in the United States is cancer related (1). It is estimated there will be 1,658,370 new cancer cases in 2015 in the United States alone, with an estimated 589,430 cancer related deaths (excluding basal cell and squamous cell skin cancer and *in situ* carcinoma except urinary bladder cancer) (1). However because of earlier diagnoses and improved therapies, the five-year relative survival rate for all cancers in 2004-2010 was 68% as compared to only 49% in 1975-1977 (1). Based on these statistics, there is still a need for new and improved cancer therapies.

The original purpose of this study was to identify selective small-molecule inhibitors of cytoplasmic dynein. Cytoplasmic dynein is the major minus-end (towards the nucleus) microtubule-associated-transport protein (2). Along with transporting various cargoes, cytoplasmic dynein is also involved in several mitotic functions such as nuclear envelope breakdown, centrosome positioning, and cytokinesis (3). A previous study has shown that knockdown of cytoplasmic dynein with RNAi delays but does not completely stop mitosis (4). Based on the fact that inhibition of cytoplasmic dynein only slows mitosis and does not completely stop it (4), an inhibitor of cytoplasmic dynein may be beneficial in the treatment of

fast growing tumors and may produce fewer side effects than microtubule perturbagens such as paclitaxel. When this study began there were no known selective small-molecule inhibitors of cytoplasmic dynein. In 2012, the first selective inhibitors of cytoplasmic dynein were identified and as of 2015, no new inhibitors have been published, giving rise to the need for novel cytoplasmic dynein inhibitors (5). Utilizing a high-content screen (HCS) focused on inhibition of GR-translocation, it was possible to test a chemical library for inhibitors of hsp90 and cytoplasmic dynein simultaneously, among multiple other possible targets.

HCS is a technique used by researchers to measure a given biological activity or phenotype in cell populations after treatment with thousands of agents such as small-molecules, peptides, and RNAs. The use HCS was first mentioned in a 1997 publication by Guliono *et al* in which they explored this new technology for the purpose of drug discovery (6). HCS provides researchers with the ability to measure multiple properties or features of the cells concurrently by measuring fluorescent signals simultaneously in multiple channels. This is in contrast to high-throughput screening providing only a single readout of activity (7) In 1999 Dr. Gordon Hager and his group at the National Cancer Institute developed a mouse adenocarcinoma cell line (3617.4 cell line) that stably overexpress a rat glucocorticoid receptor attached to a green fluorescent protein (GR-GFP) in order to visualize the translocation of the glucocorticoid receptor (GR) from the cytoplasm to the nucleus (8). Using an HCS assay developed in this cell-line, researchers can simultaneously visualize the GR-GFP and the nucleus using Hoechst to stain nuclear DNAs, and can measure GR-agonist induced translocation of GR from the cytoplasm into the nuclear compartment of the cell (9). A HCS campaign to identify inhibitors of dexamethasone-induced GR-GFP nuclear translocation in 220,000 compounds from the NIH

molecular library screening center network (MLSCN) compound library was conducted by the University of Pittsburgh Molecular Library Screening Center (PMLSC, http://pmlsc.pitt.edu/) in the University of Pittsburgh Drug Discovery Institute (9). 3617.4 cells were seeded into assay plates and incubated for 48 hrs in Tet-free media to induce GR-GFP expression and were then pre-exposed to 20 μM of the compound library for 1 hr prior to a 30 min treatment with 1 μM dexamethasone to induce GR-GFP translocation into the nucleus. Any compound that inhibited one or more component of GR translocation would inhibit the translocation. Positive and negative controls included cells that were there treated and not treated with dexamethasone respectively. 17-AAG, an hsp90 inhibitor that has previously been shown to block the agonist-induced nuclear translocation of steroid nuclear receptors including GR, was used to validate the GR-GFP translocation assay during development of the HCS assay (9,10). Two fluorescent channels were independently acquired by the automated fluorescence imager; GR-GFP in the FITC channel and Hoechst stained nuclei in the DAPI channel . Nuclear and cytoplasmic regions were trained into a molecular image analysis algorithm by user-defined thresholds; described in detail in the 'METHODS" section of chapter 2. The molecular image analysis algorithm calculated translocation of the GR-GFP by subtracting the mean average GR-GFP intensity in the cytoplasmic ring region from the GR-GFP intensity in the nuclear region to produce a mean circ-ring intensity difference (9, 10).

The GR is a ligand-activated transcription factor that belongs to the nuclear receptor superfamily, one of the most abundant classes of transcriptional regulators in animals (11). GR regulates a variety of physiological functions such as metabolism, development, differentiation, and reproduction (12). In the absence of glucocorticoid steroid the GR is primarily found in the cytoplasm existing as a large complex bound to chaperone proteins hsp90, hsp70, hsp40, hsp

organizer protein (Hop), p23 and immunophilins. GR is in a ligand competent state when bound in this heterocomplex (13). The conformational changes brought about by hsp90-hsp70-hsp40-Hop in the complex allow the ligand-binding pocket to be open and available to bind glucocorticoid steroids (Figure 1). This complex binds the GR, and the binding of ATP by hsp90 causes a conformational change in the GR to the "open" position in its ligand-binding domain (LBD), allowing the GR to bind glucocorticoid steroid (14). After the GR LBD is in the open confirmation and ready to accept glucocorticoidsteroid, Hop and hsp70 leave the heterocomplex and p23 binds and stabilizes the heterocomplex. In the heterocomplex Hop is bound to the tetratricopeptide repeat (TRP) domain of hsp90 and after its release the hsp90 TRP domain binds the immunophilin FKBP52. The GR heterocomplex is then linked to cytoplasmic dynein via a protein-protein interaction with FKBP52 (Figure 2). Upon glucocorticoid binding, the GR is activated and rapidly transported from the cytoplasm to the nucleus along microtubules by cytoplasmic dynein where it binds to DNA and regulates the transcriptional activity, either positively or negatively, of its target genes (13, 14).

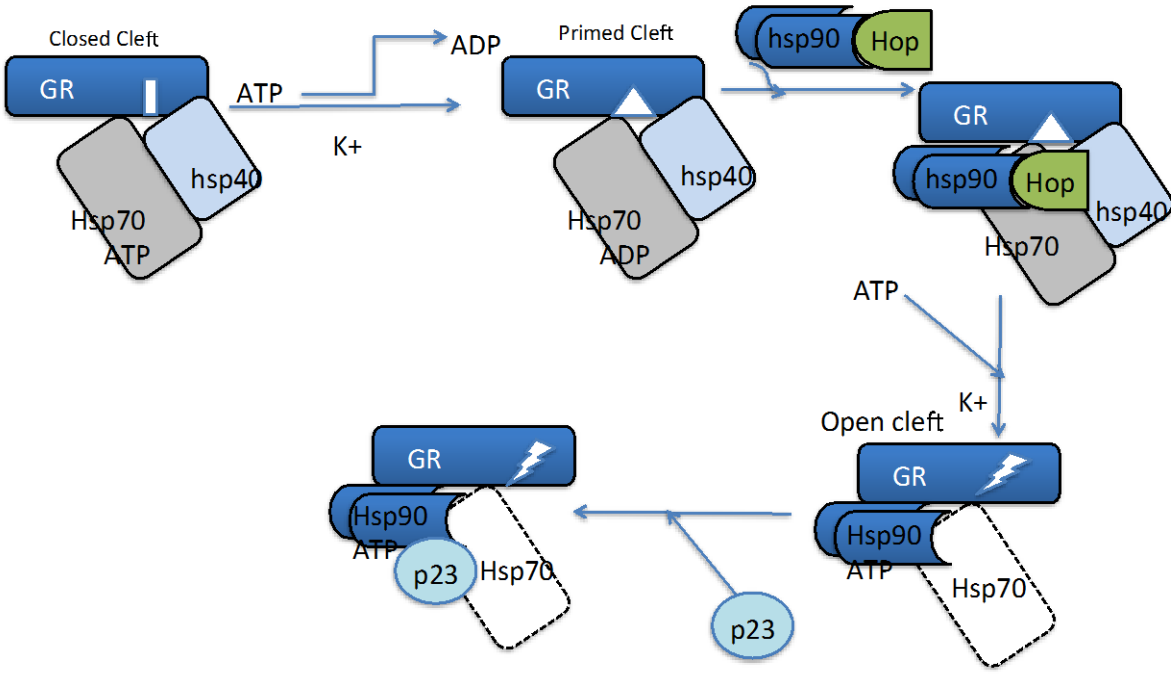

Figure 1: GR Ligand-Binding Domain (cleft) Opening by Hsp70 and Hsp90
Hydrolysis of ATP by hsp70 bound in the GR hetero-complex primes the complex to be ready to bind hsp90. Once bound to the hetero-complex, hsp90 binds ATP causing a conformational change that opens the ligand binding domain, making it ready to bind glucocorticoid steroid. The binding of p23 to hsp90 stabilizes the ATP bound confirmation of hsp90. Figure adapted from Pratt *et al.* (14)

The translocation of GR occurs after glucocorticoid steroid binding to the LBD of GR maintained in a high affinity binding state by ATP-bound hsp90 in a hetero-complex that includes hsp70, hsp40, Hop, and p23.. After glucocorticoid steroid is bound to GR, the GR attaches to cytoplasmic dynein and is transported from the cytoplasm to the nucleus. Inhibition of hsp90 has been shown to inhibit translocation of the GR (9,10, 14). Since GR is one of the cargos transported by cytoplasmic dynein, it is also likely that inhibition of cytoplasmic dynein would inhibit GR-translocation (10). Because the translocation of GR from the cytoplasm to the

nucleus depends on the activity of both hsp90 and cytoplasmic dynein it is possible that a sub-set of hit compounds from the HCS might be hsp90 or cytoplasmic dynein inhibitors. Compounds inhibiting GR-translocation could also be inhibiting a number of other proteins such as hsp70, hsp40, Hop, p23, immunophilins, and alpha and beta importins. Another possibility is that a sub-set of the hit compounds were antagonists of glucocorticoid steroid binding to GR.

Hsp90 is a molecular chaperone protein that is important in many cellular processes such as cell cycle control and cell survival (15). This versatile chaperone protein also aids in the function and stabilization of many proteins including oncoproteins, which makes hsp90 the target of new cancer therapies (15, 16). Cancers cells have a higher sensitivity to hsp90 inhibitors than normal cells. Hsp90 derived from cancer cells have a higher affinity for hsp90 inhibitors, most likely due to hsp90 in cancer cells being in large multichaperone-client protein complexes that differ from the complexes formed in normal cells (17). For example, hsp90 derived from cancers cells have 100-fold higher affinity for the hsp90 inhibitor 17-AAG than hsp90 derived from normal cells (17). Recently, several hsp90 inhibitors have failed in clinical trials for reasons ranging from poor pharmacokinetic properties to manufacturing difficulties, thus creating a need for novel hsp90 inhibitors (3).

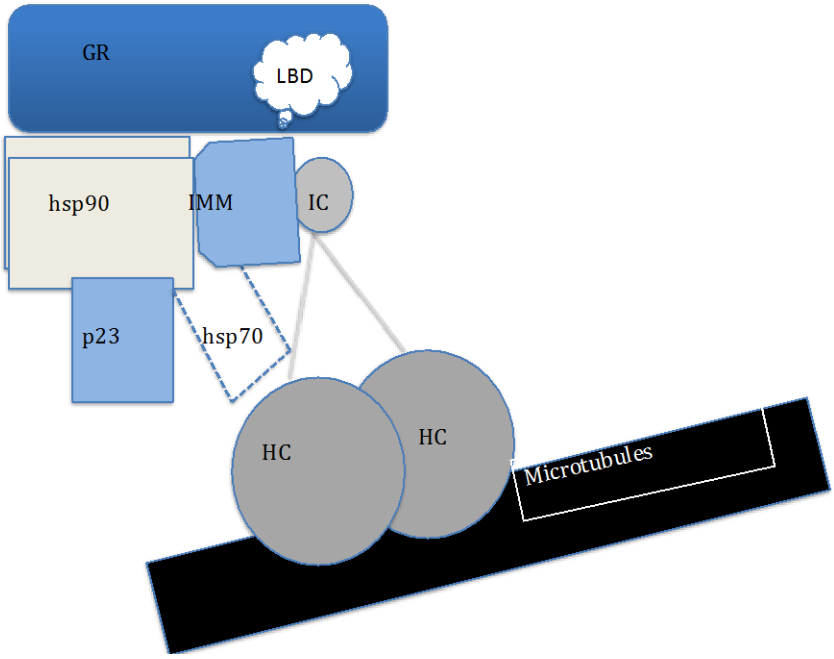

Figure 2: The GR-hsp90-immunophilin Complex Attaches to Cytoplasmic Dynein for Retrograde Transport Along Microtubules Towards the Nucleus.

Hsp70 is drawn with a dotted line because once the GR LBD is in the open position Hop and hsp70 leave the hetero-complex, however small amounts of hsp70 stay weakly bound. Once Hop and most of hsp70 leave the hetero-complex p23 stabilizes the hsp90 dimer. IC: intermediate chain dynein; HC: heavy chain dynein; IMM: immunophilin FKBP52; GR: glucocorticoid receptor; hsp90: heat-shock protein 90. Figure adapted from Pratt et al 2004 (14)

In eukaryotes there are three main families of cytoskeletal motor proteins: myosins, kinesins, and dyneins (2, 3). Prokaryotes have different motor proteins. All of these families of protein utilize the hydrolysis of ATP to ADP to power their motor protein domain and thus their movement along cytoskeletal polymers. Myosins travel along actin filaments; kinesins and dyneins travel along microtubules (3). The transport of cargo differs between dynein and kinesin in that dynein travels towards the minus-end of microtubules , whereas most kinesins (with the exception of the kinesin 14 family) travel towards the plus-end of microtubules (away from the nucleus) (2).

Two classes of dyneins, axonemal and cytoplasmic dynein, have been identified. Of these there have been 13 forms identified as axonemal and only two forms identified as cytoplasmic dynein (18). Axonemal dyneins are anchored within the axoneme and aid in the coordinated beating of cilia and flagella (19). The two forms of cytoplasmic dynein, cytoplasmic dynein 1 and dynein1b (also known as intraflagellar transport dynein), have very different distributions and range of function. Dynein 1b has a specific and restricted cellular distribution, primarily expressed in ciliated epithelial cells, and a limited range of function, while dynein 1 has a wider cellular distribution with multiple functions (18). Cytoplasmic dynein 1 is involved in transport of organelles, mRNAs, and proteins as well as several mitotic functions such as nuclear envelope breakdown, centrosome positioning, and cytokinesis (3, 18).

All dyneins are found in a multi-subunit complex and each form of dynein contains a conserved heavy chain (HC) (Molecular weight >500 kDa) (18). Cytoplasmic dynein HC is found as a homodimer linked by the N-terminal tail (19). The motor domain of the HC of dynein consists of six ATPase Associated with diverse cellular Activities (AAA+) domains. The AAA1 and AAA3 domains carry out most of the ATP hydrolysis (20). The AAA2 and AAA4 domains can also bind ATP, but AAA5 and AAA6 have lost their nucleotide binding sites (19, 20). Many subunits of dynein associate with the heavy chain on the N-terminus tail such as light chains, light intermediate chains, and intermediate chains of dynein (19). These proteins, as well as other proteins and a complex named dynactin, are vital for the association of cytoplasmic dynein to cargo (19, 21). Dynactin is a multi-protein complex that enhances dynein's mobility along microtubules and serves as an adaptor that allows dynein to bind cargo and these proteins are also possible targets of the phenotypic GR-GFP nuclear transport assay (22). Two major protein subunits of dynactin are $p150^{Glued}$ and dynamitin. Dynein attaches to dynactin through an

interaction between the dynein intermediate chain and $p150^{Glued}$. $P150^{Glued}$ also binds microtubules, which not only stabilizes dynein's attachment to microtubules, but also increases the rate at which dynein moves along microtubules (22). Dynactin exists in multiple protein subunits that are linked together by dynamitin. Overexpression of recombinant dynamitin inhibits dynein transport by destabilizing the endogenous structure of dynactin (21). Before the discovery of the first selective small-molecule inhibitors of cytoplasmic dynein (ciliobrevin A and D) in 2012, the only tools available to researchers to inhibit cytoplasmic dynein were antibodies specific for dynein light and intermediate chains and overexpression of dynamitin (5) Varying protein compositions of the pointed end of dynactin are thought to determine the cargo that will associate with the complex and therefore be transported by dynein. The subunit pairs p62/Arp11 and p27/p25 allow dynactin to bind different cellular components during different stages of the cell cycle. This is important to allow dynein to drive the distinctly different types of motility required during interphase and at the beginning of mitosis (23). Yeast lack p62, p27, and p25 which suggests that many of dynactin's functions are independent of these subunits (22, 23).

To characterize the hit compounds from the HCS, they were analyzed for promiscuity using PubChem (24), a pan assay interference compounds (PAINS) database (25), a medicinal chemistry analysis using Instant JChem (24), a docking simulation against hsp90 using SYBYL (26), and an ATPase assay to verify selectivity for hsp90. The PubChem cross target query and PAINS database were used to eliminate promiscuous compounds from the hit compound list. Instant JChem was used to perform a medicinal chemistry analysis in order to identify compounds that had acceptable drug-like properties. The SYBYL software was used in a docking simulation to predict hit compounds that were likely to bind hsp90. To determine

selectivity of the hit compounds, they will be tested in the PiPer™ assay kit (enzyme coupled amplex red biochemical assay) against the ATPase activities of hsp90, myosin, and kinesin.

Myosin and kinesin are intracellular transport proteins that utilize the energy release from ATP hydrolysis to transport cargoes (2). Although similar in structure and function, myosin transports cargoes along actin filaments and kinesin transports cargoes along microtubules (2). Kinesin and myosin have very similar catalytic domain structures when observed by x-ray crystallography even though they have very different amino acid sequences (28). Both of these motor proteins move in a hand-over-hand fashion as well (2). Myosin was chosen as a protein to evaluate the selectivity of hit compounds not only because it is an ATPase (hsp90 and cytoplasmic dynein are also ATPases), but also because purealin, a novel compound isolated from the sea sponge *Psammaplysilla purea*, inhibits cytoplasmic and axonamal dynein and myosin, but does not inhibit other ATPases. Purealin inhibits dynein and myosin without competing for the ATP binding site (29). Both apomorphine enantiomers, R and S, inhibit both cytoplasmic dynein and myosin with similar IC_{50}'s (10). Based on these findings, an inhibitor of cytoplasmic dynein may also inhibit myosin, and it would be important to verify that a compound found to inhibit cytoplasmic dynein does not also inhibit myosin. The fact that myosin is an ATPase also makes it a good choice to test the selectivity of compounds inhibiting hsp90. Kinesin is also an ATPase, which makes it a good choice to test against inhibitors of hsp90 and cytoplasmic dynein. Kinesin is a microtubule associated protein like cytoplasmic dynein and inhibition of either protein may occur by inhibition of microtubule binding, a mechanism that can be examined if ATPase inhibition is ruled out as the mechanism of inhibition. Kinesin and dynein are not structurally similar, but they do both bind microtubules (4). Hit compounds that inhibited GR translocation can be characterized as selective inhibitors

of hsp90, cytoplasmic dynein, myosin, or kinesin ATPase activity. A compound that inhibits either hsp90 or cytoplasmic dynein's ATPase activity and not myosin or kinesin's ATPase activity would be considered a selective inhibitor of hsp90 or cytoplasmic dynein.

1.2 HSP90

Hsp90 is a molecular chaperone protein that is ubiquitous and abundant in many cell types (15). It plays an important role in many cellular processes including cell cycle control, cell survival, hormone and other signaling pathways (15). Hsp90 interacts with proteins (clients) and is responsible for their maturation and activation (30). Many hsp90 clients are kinases or transcription factors, such as the GR. Recently it has been suggested that up to 10% of all proteins require hsp90 to function (31).

Hsp90 has three main structural domains: an N-terminal ATP binding site, a middle domain connected to the N-terminal domain via variable charged linkers, and a C-terminal domain responsible for dimerization (32) (Figure 3). The N-terminal domain of hsp90 binds ATP quickly, but with low affinity. The rate-limiting step of hsp90's ATPase activity is the hydrolysis of ATP (33, 34). ATP binding and hydrolysis are essential for the function of hsp90 (35). Although it was originally thought that the linker region between the N-terminal domain and the middle domain was just a spacer, recent studies have suggested that this linker region can modulate the activity of hsp90 (32, 36). Upon ATP binding the N-terminal domain of hsp90, dimerization occurs at the C-terminal domain. The C-terminal domain can then bind TPR

proteins, such as immunophilins, on its MEEVD motif (32) (Figure 3). Hsp90 is functional as a chaperone protein once it binds client proteins and forms a dimer. Yeast hsp90 (hsc82) was chosen as the hsp90 to test ATPase activity in this study due to the fact that it has 10-fold higher activity than that of human hsp90 and to take advantage of previously established expression and purification techniques available through the Brodsky lab (20).

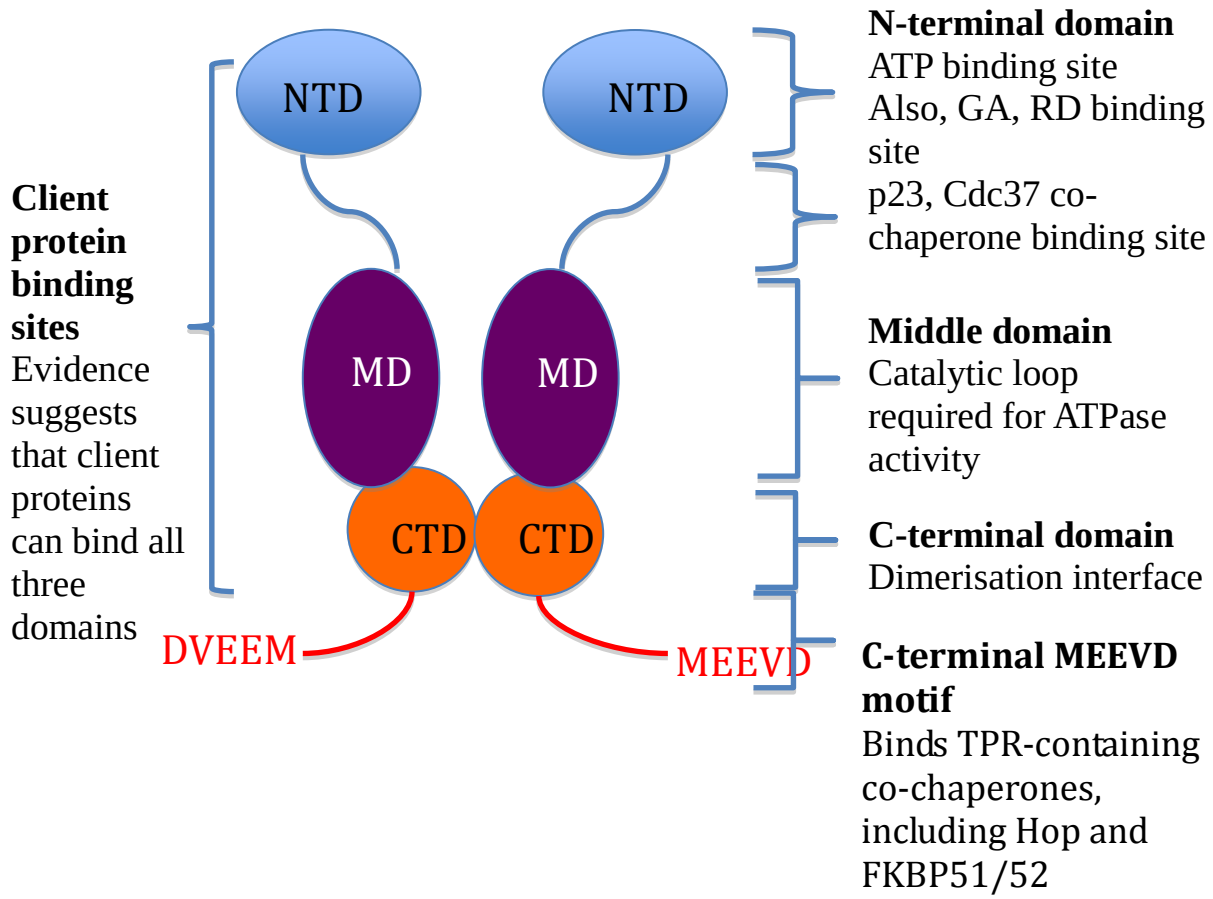

Figure 3: Structure of Hsp90

The N-terminal domain of hsp90 contains the ATP binding site. Upon ATP binding dimerization occurs at the C-terminal domain. This is linked to the middle domain by a variable charged linker region. The Middle domain of hsp90 contains the catalytic loop required for ATPase activity. The C-terminal domain is where dimerization occurs. At the end of the C-terminal there is a MEEVD motif where Hop and immunophilins bind. NTD=N-terminal domain; MD = Middle Domain; CTD=C-Terminal Domain Figure adapted from Jackson 2013 (32)

1.3HSP 90 AS A DRUG TARGET

Hsp90 is a well-known target for anti-tumor and anti-proliferative drugs, and has also been shown to sensitize cells to the toxic effects of both chemotherapy and radiotherapy (16). Cancer cells have been found to have a higher sensitivity to hsp90 inhibitors, which accumulate at higher concentrations in cancer cells as compared to normal cells (17). Hsp90 inhibitors may accumulate in higher concentration in cancer cells because cancer cells express much more hsp90 than normal cells. It could also be due to the fact that the hetero-complexes of hsp90 expressed in cancer cells have an increased affinity for hsp90 inhibitors (32). Hsp90 derived from tumor cells has been found to have 100-fold higher binding affinity to 17-AAG (hsp90 inhibitor) than that derived from normal cells (17). This makes hsp90 an excellent target for cancer therapies in that the inhibitors are likely to have more of an effect on cancer cells than normal cells. Several hsp90 inhibitors have progressed to clinical trails, though none have FDA approval due to poor drug-like properties, off target toxicity, and manufacturing issues (16). The control inhibitor of GR-translocation used to validate the original HCS was 17-AAG, an hsp90 inhibitor, so it is possible that some of the hit compounds identified in the screen could be novel hsp90 inhibitors.

2.0 GR-GFP TRANSLOCATION ASSAY

2.1 INTRODUCTION

The original high content phenotypic cell-based screen was carried out with the goal of identifying novel inhibitors of Dex-induced GR trafficking, of which cytoplasmic dynein and hsp90 inhibitors are a possible subset. However, as the results in this chapter show, the recently identified cytoplasmic dynein inhibitors ciliobrevin A and D were unable to inhibit Dexamethasone-induced GR-GFP translocation. Hsp90 inhibitors 17-AAG and STA-9090 and microtubule perturbagens vinblastine, vinorelbine, cabazitaxel, ixabepilone, doclitaxel, paclitaxel, and vincristine were also tested in the GR-GFP translocation assay as well as a novel hsp70 inhibitor, Mal3-101, that was provided by the Brodsky lab, University of Pittsburgh. After efforts to purify cytoplasmic dynein failed and based on previous observations that 17-AAG inhibited Dex-induced GR-GFP translocation (9, 10) the focus of this project was shifted to focus primarily on identifying novel inhibitors of hsp90.

Hit compounds were identified in the HCS by their ability to inhibit dexamethasone-induced GR translocation into the nucleus. Compound identities were then confirmed using liquid chromatography and mass spectroscopy (LC-MS) to confirm that the expected molecular weight species was present and the percent purity was $\geq$ 90%. Activity was confirmed by retesting hit compounds in the GR translocation assay. IC_{50}s were then determined and the hit

compound list was reduced by IC_{50} cut-offs of 10μM and 8μM. The structures of the hit compounds were also analyzed for reactivity and ease of synthesis.

2.2 Specific Aim

The goal of this aim was to identify which target protein involved in the GR-GFP translocation assay would be best to concentrate on to identify a small-molecule inhibitor for from the list of 112 hit compounds from the original screen. In the original screen hit compounds were identified from a scaffold diverse library of over 220,000 compounds from the NIH's Molecular Libraries Screening Centers Network library. The cell-based high content screen involved mouse adenocarcinoma cells that express a GR-GFP construct using a tet-repression system (tetracycline in the media inhibits expression of the construct). This assay allows us to visualize the transport of the GR by cytoplasmic dynein towards the nucleus in the presence of compounds and the GR agonist dexamethasone.

2.3 METHODS

Inhibitors of hsp90, hsp70, microtubules, and dynein were tested for their ability to inhibit GR translocation using the original high content/information assay using a 3617.4 mouse mammary adenocarcinoma cell line that expresses a rat GR-GFP construct controlled by a tet-off system (8). Cells were grown to 70% confluency in Duldecco's Modified Eagle Medium (DMEM) containing 1X nonessential amino acids, 1X sodium pyruvate, 1X penn/strep, 10% fetal bovine serum (FBS), 10μg/mL tetracycline, and 0.96mg/mL G418 in an incubator at 37°C,

5% CO_2, and 95% humidity. Once at 70% confluency, determined visually under a microscope, the cells were washed with DMEM containing all the components from the growth media (listed above) with the exception of no tetracycline and charcoal-filtered FBS instead of normal FBS. Cells were harvested by trypsinization followed by centrifugation at 500 x g for five minutes and re-suspendion in tet-free media. Viable cells, determined by the exclusion of trypan blue, were counted in a hemocytometer. Cells were seeded at 2,500 cells per well in a 384-well plate and incubated for 48 h in DMEM media at 37°C, 5% CO_2, and 95% humidity. After 48 h the cells were treated with inhibitors of hsp90, hsp70, microtubules and dynein at a final concentration of 20μM and incubated at 37°C for 1, 3 or 24 hours. The cells were then treated with a concentration of dexamethasone (100nM) that causes a 100% increase in nuclear GFP accumulation (as determined by a dexamethasone titration) and incubated for 30 min at 37°C. Following dexamethasone treatment, cells were fixed with 3.7% formaldehyde and stained with a Hoechst stain (2μg/mL). After incubation at room temperature for 30 min, fluorescence images were acquired using the ImageXpress Micro automated high content imaging platform (Molecular Devices LLC, Menlo, CA) (9).

The translocation enhanced image analysis algorithm defined the nucleus of each cell as objects that exhibited a fluorescent intensity in the DAPI channel (Hoechst channel) that were above background and the appropriate size, defined using the ImageXpress software tools to measure nuclear diameters, areas, and intensities over background. . The nuclear inner mask was eroded by 1 pixel to reduce cytoplasmic contamination of the GR-GFP channel (FITC) in the nuclear area in order to quantify the amount of GR-GFP signal in the nucleus. The cytoplasmic outer region was defined by dilating the nuclear mask through the cytoplasm as much as possible without moving outside of the cellular boundary and then subtracting the original nuclear region.

The width of the cytoplasmic outer region was 3 pixels. This cytoplasmic outer region was then used to quantify the amount of GR-GFP signal in the cytoplasm. The translocation enhanced image analysis algorithm quantifies the cell count through the DAPI channel and the average fluorescent intensities of the nuclear (Inner) and the cytoplasm (Outer) regions. To calculate the translocation of GR-GFP from the cytoplasm to the nucleus the algorithm calculated a mean average intensity ratio by dividing the average GR-GFP intensity of the Inner region by the average GR-GFP intensity of the outer region (9, 10).

Optimal assay conditions for the GR-GFP translocation assay were determined experimentally before testing the inhibitors in the assay (9). For the first optimization step plates containing dexamethasone treated cells were either aspirated first and then treated with formaldehyde or treated with formaldehyde and then aspirated to determine the order producing the optimal results (Figure 5). The next optimization step was to determine the optimal time to treat the cells with dexamethasone. Cells were treated with dexamethasone and then fixed at 0, 5, 10, 20, 30, 60, 90, and 120 minutes and then read on the IXU platform (Figure 6). The final optimization step was to determine the optimal concentration of dexamethasone the cells should be treated with to insure maximal translocation (Figure 7). Cells were treated with serial dilutions of dexamethasone in the range of 1×10^{-4}nM to 1×10^{2}nM.

2.4 Results

A. Optimization of GR-GFP Translocation Assay

Figure 4 presents representative color composite fluorescent images of 3617.4 cells cultured for 48 hours in tet-free media and then treated for 30 min with 100nM dexamethasone + 0.5% DMSO (Figure 4B) or media containing 0.5% DMSO without dexamethasone (Figure

4A). In cells treated with 0.5% DMSO, minus dexamethasone, the GR-GFP appears to be found predominately found in the cytoplasm of the 3617.4 cells (Figure 4A). In contrast, cells treated with 100nM dexamethasone for 30 minutes the GR-GFP was almost exclusively localized within the nuclear region (Figure 4B). Each optimization step was carried out in triplicate and on three separate days, each figure is the best representations of each. Figure 5 compares the results of aspirating or fixing first to determine the order giving the most consistent results. Comparing the two orders it is apparent that is it is not important which is done first, aspirate or fix. The next optimization step was to determine how long the cells should be treated with dexamethasone before they are fixed with formaldehyde (Figure 6). Maximumal GR-GFP translocation was accomplished at 20 minutes. Based on those results, 30 minutes was determined to be the optimal exposure time for dexamethasone prior to fixing cells in formaldehyde to reduce variation between experiments. The final optimization was to determine the optimal concentration of dexamethasone to use (Figure 7). The goal was to find a concentration that was well into the maximal translocation range. Based on the results shown in figure 7, it was determined that 100nM dexamethasone should be sufficient to attain maximal GR-GFP translocation. The EC50 was calculated to be approximately 0.92nM, which is consistent with previously published results (9)

A B

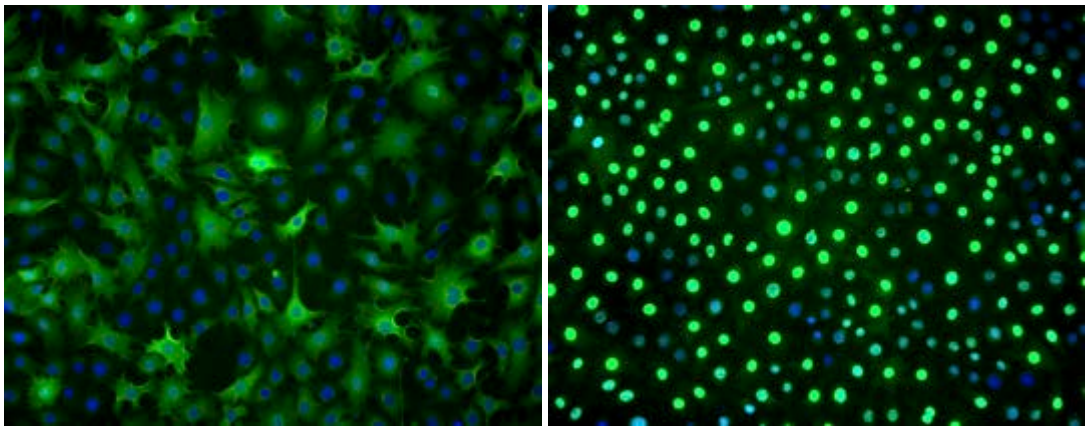

Figure 4: Color Composite Images of Dexamethasone Treated (B) and Untreated (A) 3617.4 Cells
Representative images presented here are from one of 3 separate experiments performed on three separate days.
Color composite images of GR-GFP (green) and the Hoechst stained nuclei (blue). Before treatment with dexamethasone the GR-GFP is predominantly located in the cytoplasm. After dexamethasone treatment (100nM) the GFP is found primarily in the nucleus.

A

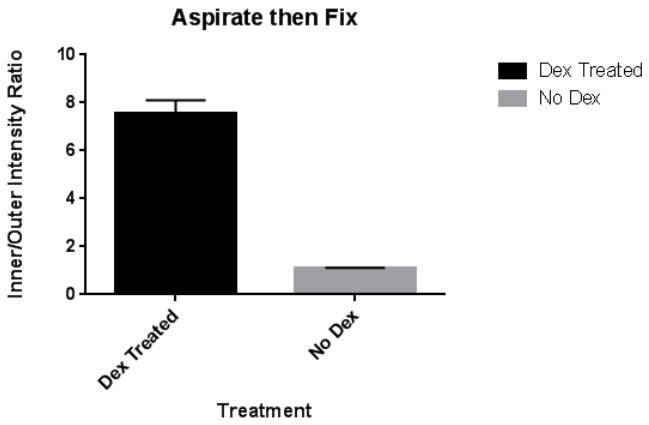

B

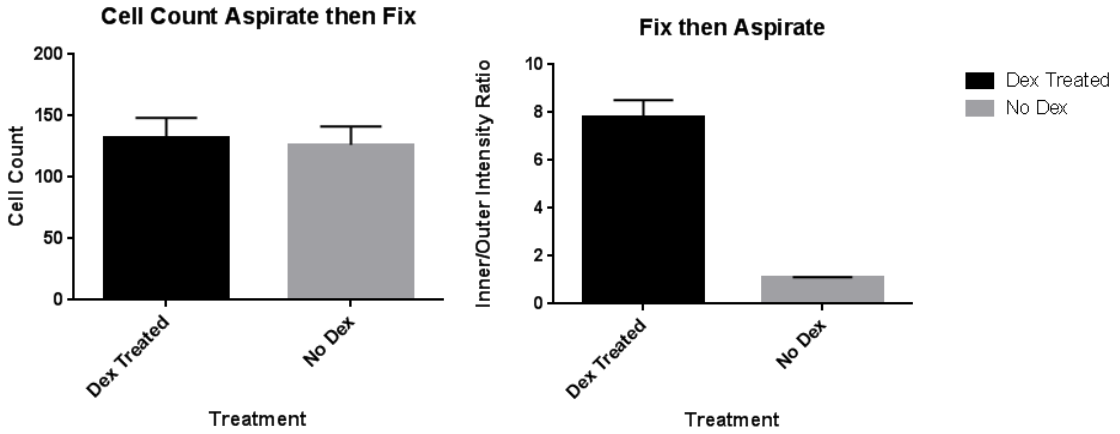

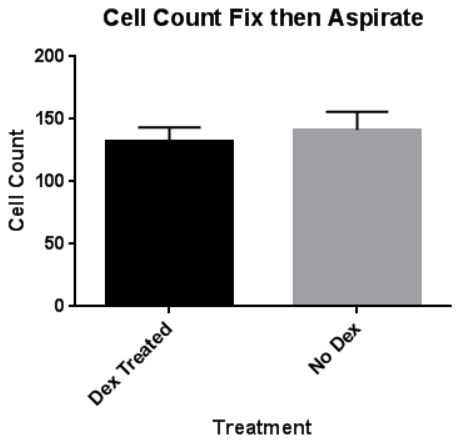

Figure 5: Determine Order of Aspiration and Fixation for Dexamethasone-induced GR-GFP Nuclear Translocation.
3617.4 Cells expressing GR-GFP were treated for 30 minute with 100nM dexamethasone (dex) or no dex and treated with 3.7% formaldehyde either before (B) or after (A) aspiration of media. The error bars represent standard deviation. Each treatment was completed in triplicate. The Y-axis is the inner/outer ratio calculated by dividing the inner (nucleus) intensity by the outer (cytoplasm) intensity . Data representative of three experiments run three separate days.

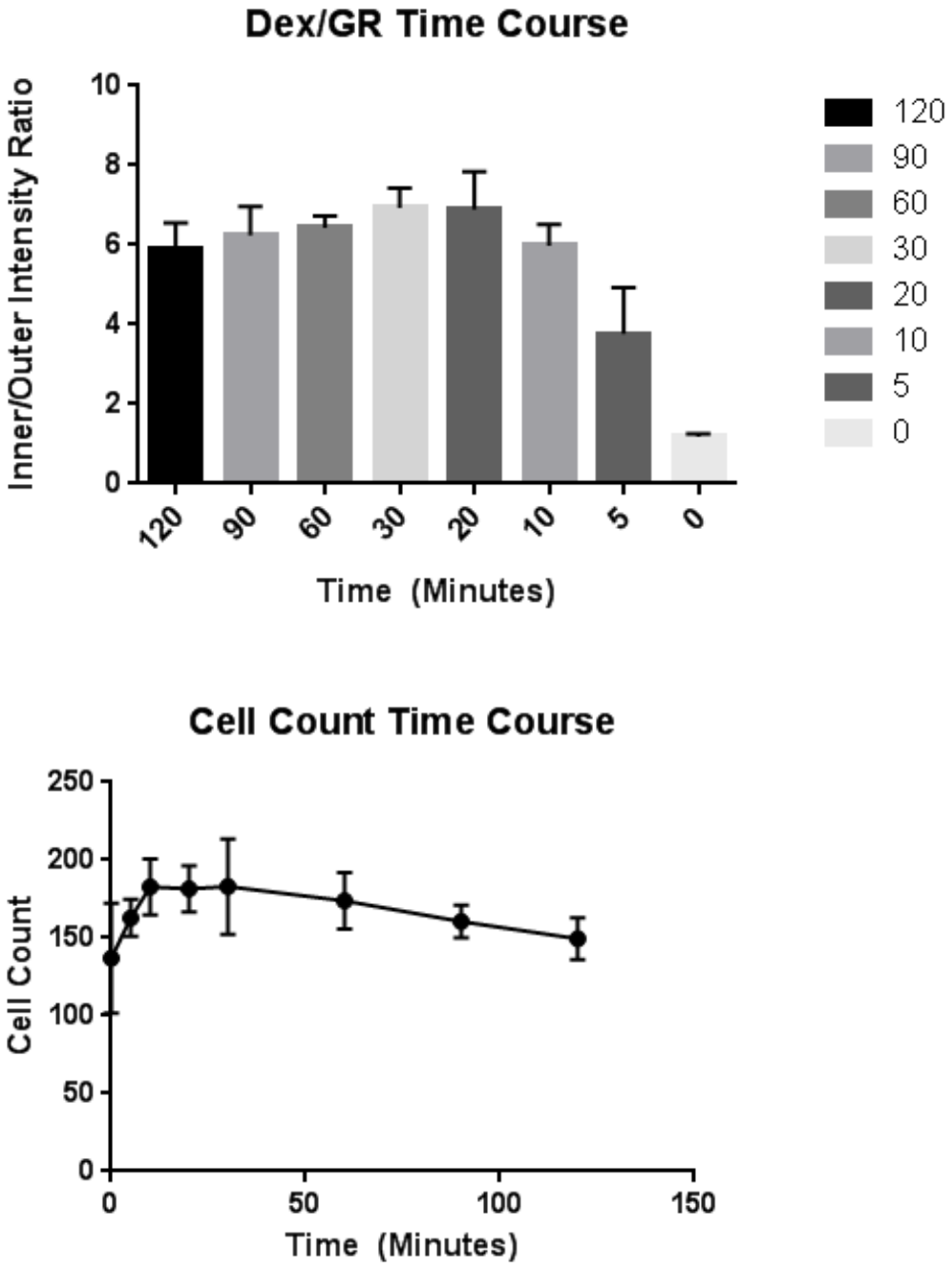

Figure 6: Time Course of Dexamethasone-induced GR-GFP Nuclear Translocation

Cells were treated with 100nM dexamethasone at different incubation times and fixed at the end of each time point. The Y-axis is the Inner/Outer ratio calculated by dividing the inner (nucleus) intensity by the outer (cytoplasm) intensity. The X-axis is time in minutes
Data is representative of three separate experiments run three separate days. All treatments were run in triplicate and error bars are in standard deviation.

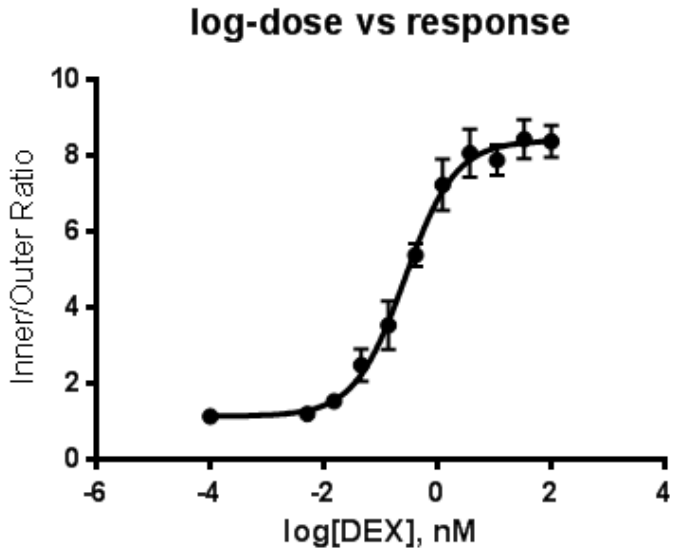

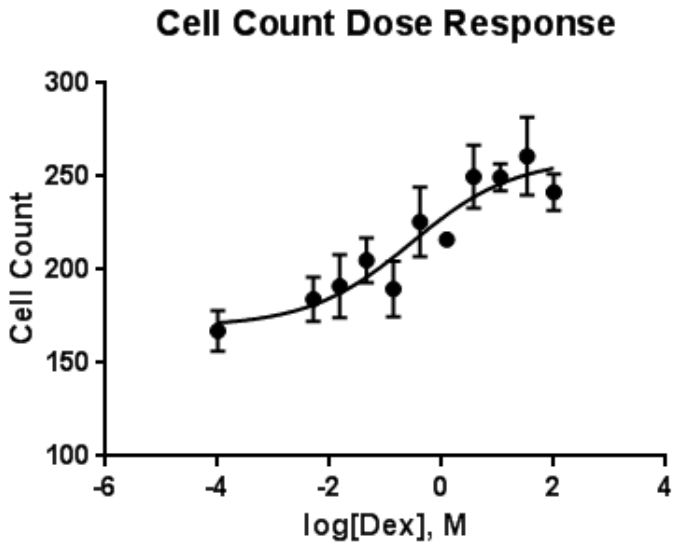

Figure 7: GR-GFP Nuclear Translocation Dexamethasone-induced Concentration Response
3617.4 cells were treated with serial dilutions of dexamethasone to determine a concentration to be used that is well in the maximal signal range. . Y-Axis is the Inner/Outer ratio calculated by dividing the Inner (nucleus) intensity by the Outer (cytoplasm) intensity. Error bars are in standard deviation. Data is representative of three separate experiments run three separate days. All treatments were run in triplicate.

B. Test Cytoplasmic Dynein, Hsp90, Hsp70 Inhibitors and Microtubule Perturbagens

The original focus of this project was to identify novel cytoplasmic dynein inhibitors. In 2012 the first selective inhibitors of cytoplasmic dynein were published (5). These compounds were named ciliobrvin A and D, because cells that are treated with them have shortened cilia(17). To test these inhibitors in the translocation assay the 3617.4 cells were treated with ciliobrevin A and D (purchased from Tocris, Bristol, UK). The results from these experiments are shown in Figures 8 and 9. Figure 8B compares the average inner intensity (nucleus) to the average outer intensity (Figure 8C) (cytoplasm) of the GFP signal in the GR translocation assay after treatment with the dynein inhibitors ciliobrevin A and D at 100μM, 75μM, 50μM, 25μM and 12.5μM for one hour prior to dexamethasone addition. Initially the inner/outer intensity ratio appeared to decrease due to increasing ciliobrevin concentrations, implying that the inhibition of GR translocation was successful when cells are treated with the ciliobrevins (Figure 8A). However, ciliobrevin A was cytotoxic (Figure 8A) and both compounds appear to fluoresce in the GFP channel (Figure 9). Their average outer intensity is equal to or higher than the

negative control and their average inner intensity is also equal to or higher than the positive control (Figure 8B). This was confirmed when cells that were still being treated with tetracycline, not producing GFP, were exposed to the compounds and there was an increase in fluorescence that appears to be concentration-dependent (Figure 9). This means that unfortunately the ciliobrevins could not be used to show proof of concept that small-molecule inhibitors of cytoplasmic dynein would inhibit Dex-induced GR-GFP translocation.

A

B

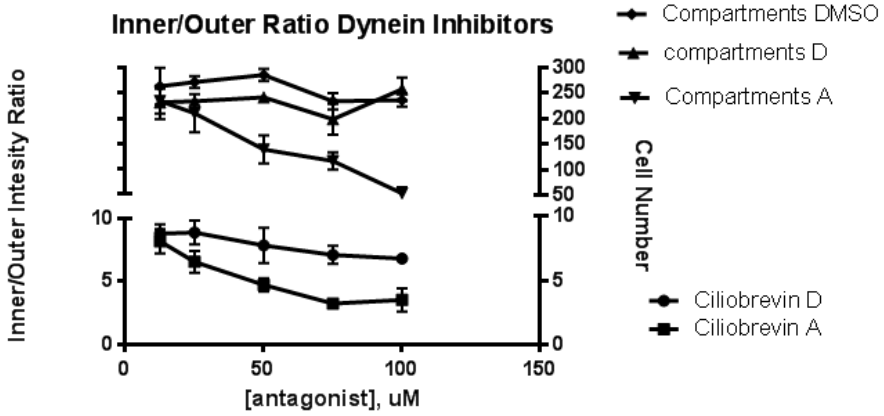

C

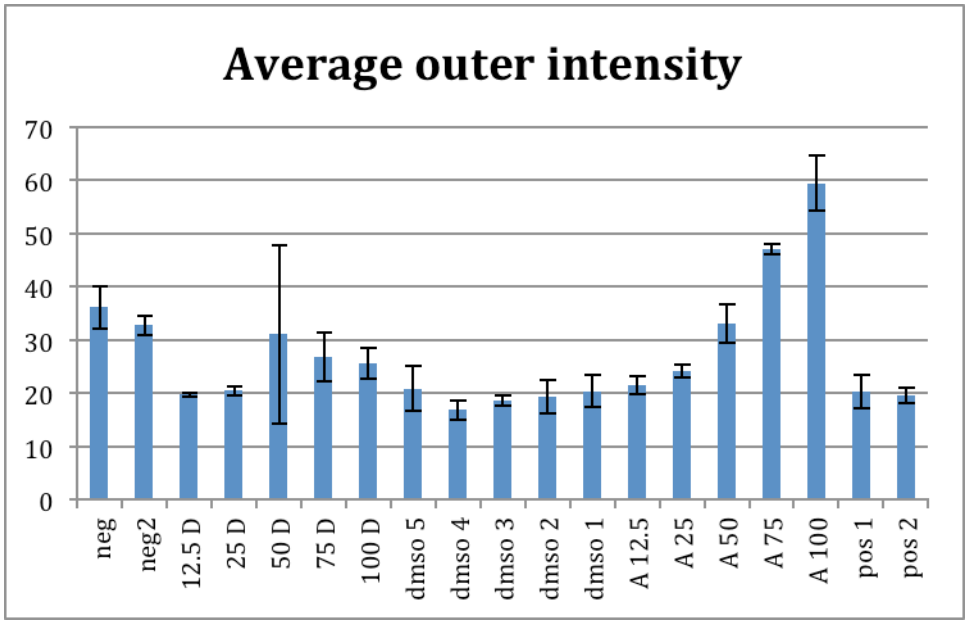

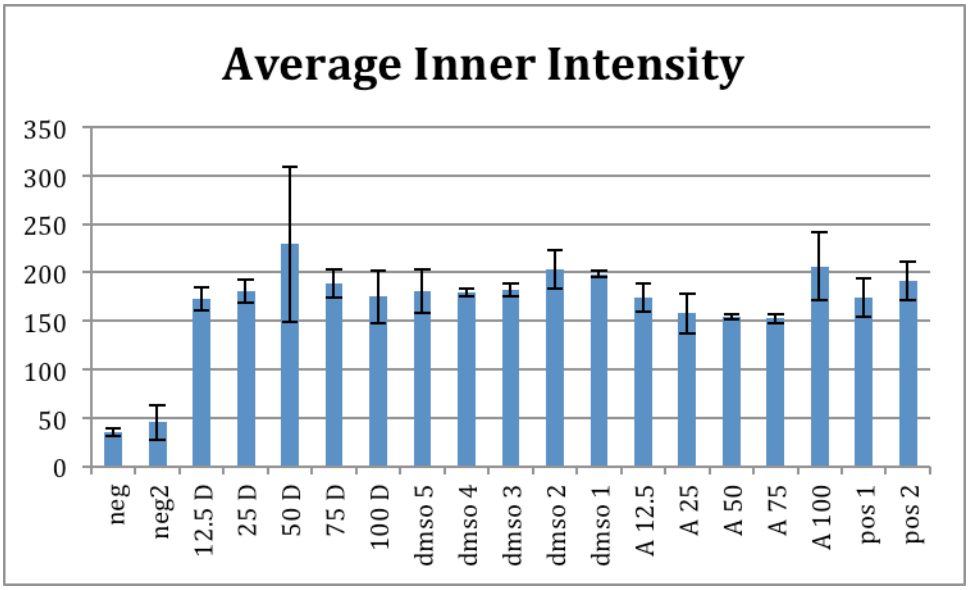

Figure 8: Inner/Outer Ratio and Average Outer and Inner Intensity of GFP in 3617.4 Cells Treated with Cytoplasmic Dynein Inhibitors

Cells were pre-treated with dynein inhibitors for one hour before the addition of 100nM dexamethasone. (A) Inner/outer ratio and cell counts. Average outer and inner intensity (B&C) Neg = negative control (no dex); Pos = positive control (dex treated); D = Ciliobrevin D (concentration 12.5, 25, 50, 75, 100μM; A= Ciliobrevin A (Concentrations 12.5, 25, 50, 75, 100μM). The graph title describes the Y-axis. Error bars are in standard deviation. Each treatment was completed in triplicate. Results depicted here are representative of three separate experiments carried out three separate days.

A

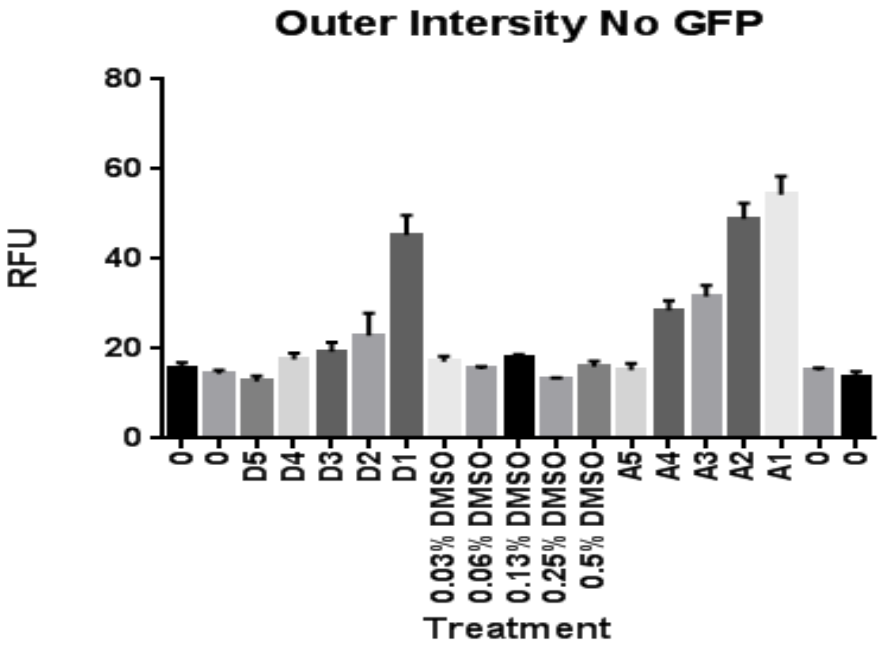
Outer Intersity No GFP
RFU
80
60
40
20
0
0
0
D5
D4
D3
D2
D1
0.03% DMSO
0.06% DMSO
0.13% DMSO
0.25% DMSO
0.5% DMSO
A5
A4
A3
A2
A1
0
0
Treatment

B

C

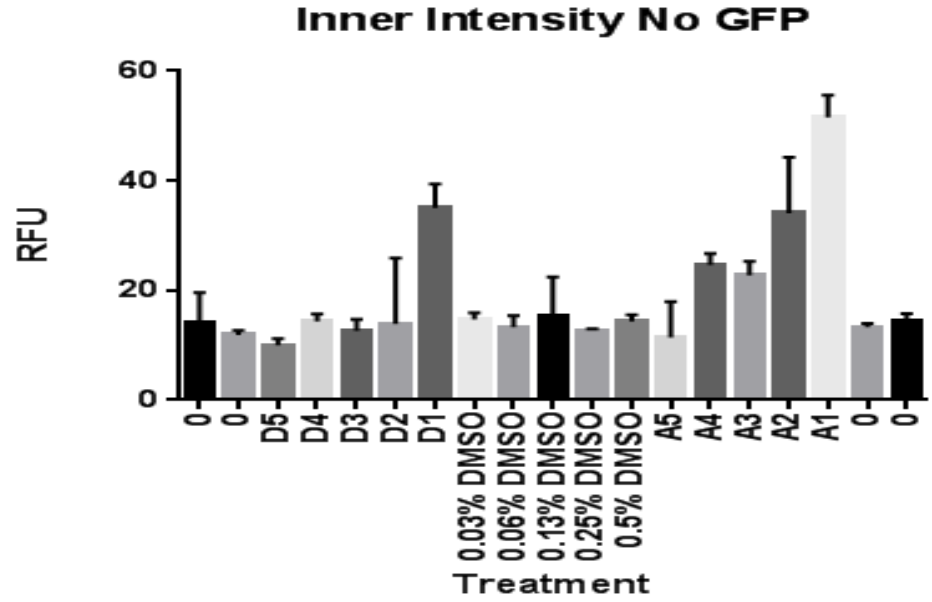
Inner Intensity No GFP
RFU
60
40
20
0
0
0
D5
D4
D3
D2
D1
0.03% DMSO
0.06% DMSO
0.13% DMSO
0.25% DMSO
0.5% DMSO
A5
A4
A3
A2
A1
0
0
Treatment

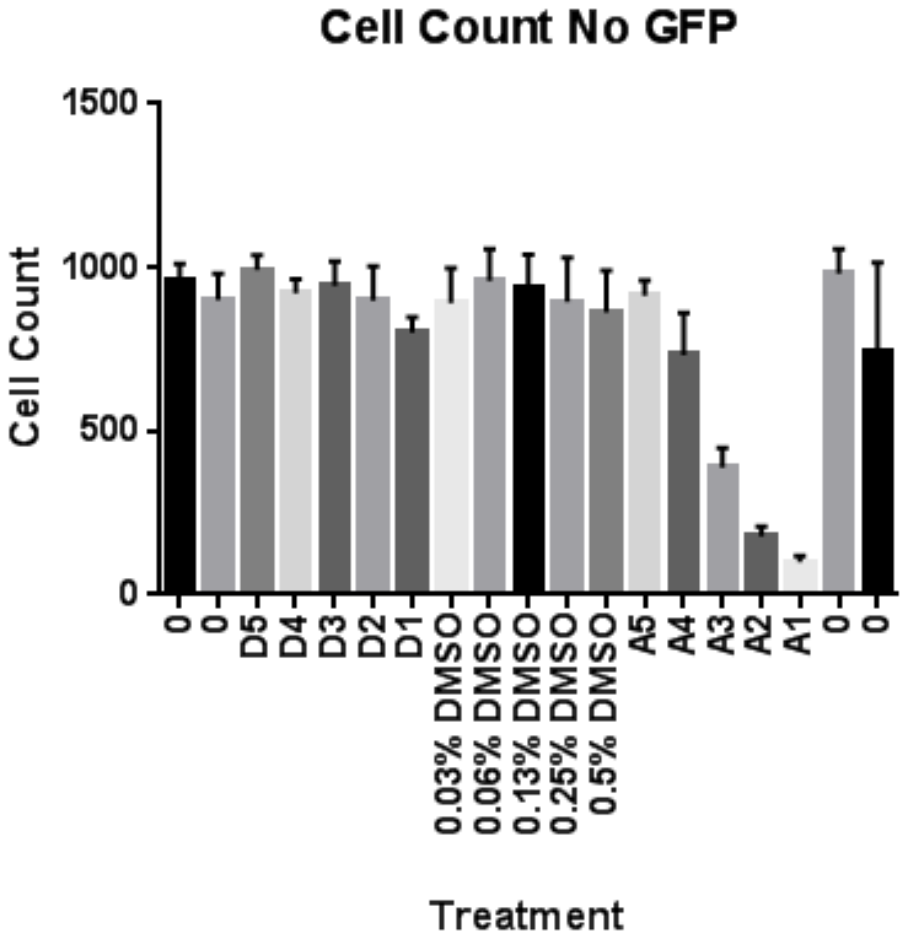
Cell Count No GFP
Cell Count
1500
1000
500
0
0
0
D5
D4
D3
D2
D1
0.03% DMSO
0.06% DMSO
0.13% DMSO
0.25% DMSO
0.5% DMSO
A5
A4
A3
A2
A1
0
0
Treatment

Figure 9: Average Outer and Inner Intensity of GFP Channel of 3617.4 Cells Treated With Cytoplasmic Dynein Inhibitors With No GFP
Best results of three separate experiments over three separate days
Error bars in standard deviation
0 = No compound added; D = Ciliobrevin D (concentration 12.5, 425, 50, 75, 100μM (5, 4, 3, 2,1 respectively)); A= Ciliobrevin A (Concentrations 12.5, 25, 50, 75, 100μM (5, 4, 3, 2,1 respectively)); RFU = Relative Fluorescence Units.

After the dynein inhibitors failed to show proof of concept, it was decided to test other possible inhibitors of GR-translocation in the GR translocation assay to determine a target where proof of concept could be shown.. Figure 10 shows the results of testing microtubule perturbagens, hsp90, and hsp70 inhibitors in the GR translocation assay. None of the microtubule perturbagens had an apparent effect on GR translocation (Figure 10), which is consistent with published results that suggest that not only is the GR transported to the nucleus via cytoplasmic dynein, but there may be alternate microtubule-independent routes (8). The novel hsp70 inhibitor MAL3-101also did not have any effect on GR translocation (Figure 10A). Consistent with the original assay development studies (9, 10), both the hsp90 inhibitors 17-AAG and STAT9090 inhibited Dex-induced GR-GFP nuclear translocation (Figure 10A). Fluorescent images of cells treated for one hour with STA9090 and paclitaxel prior to the 30 minute treatment with dexamethasone are represented in Figure 10B. The image of the cells treated with STA9090 are consistent with the image of the cells in Figure 4A, confirming that STA9090 inhibits GR translocation. Conversely, the image of the cells treated with paclitaxel

are consistent with the image of the cells in Figure 10B, confirming that paclitaxel does not inhibit GR translocation.

A

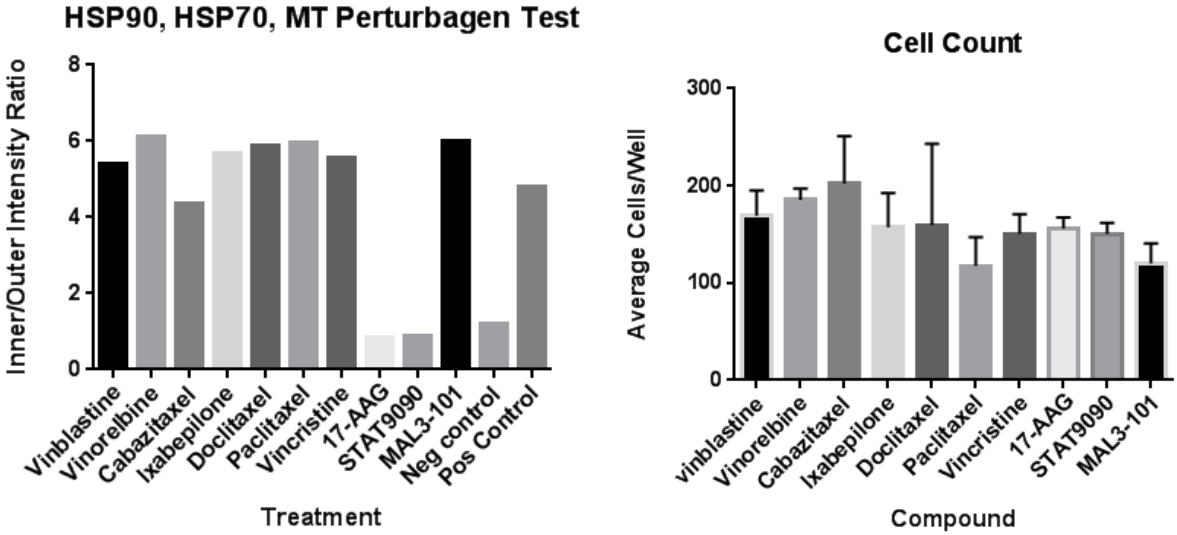

B

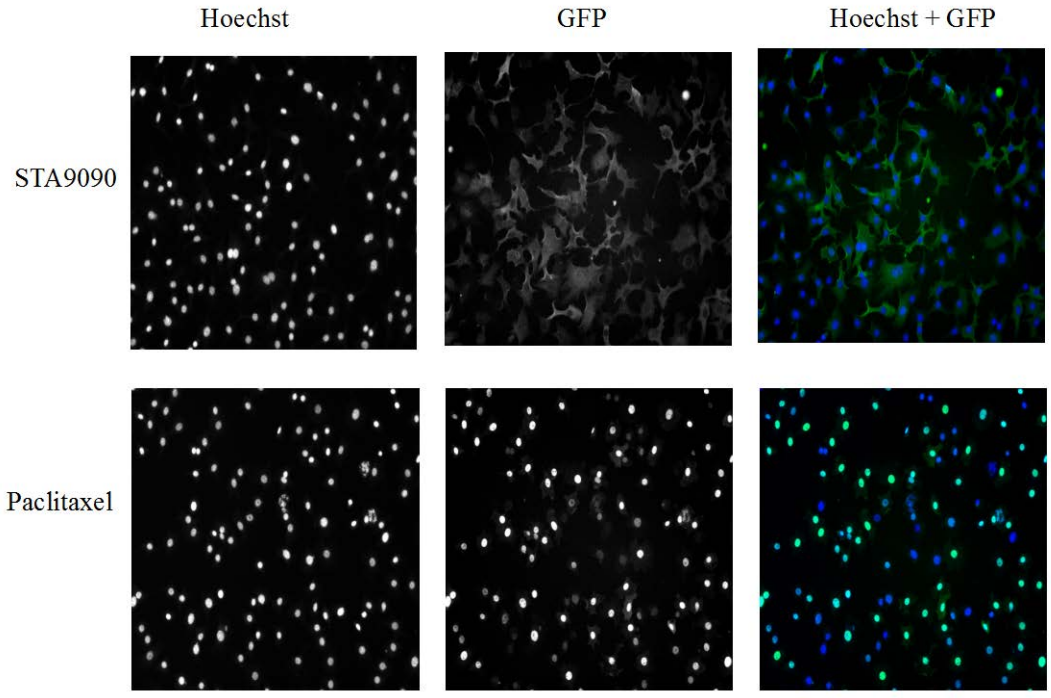

Figure 10: 3617.4 Cells Treated With Microtubule Perturbagens, Hsp90, and Hsp70 Inhibitors.
Best results of three experiments over three separate days. Error bars in std dev.

2.5 DISCUSSION

When optimizing the GR-GFP translocation assay the first step was to show that in the presence of dexamethasone the GFP co-localizes with the nucleus and without dexamethasone treatment the GFP stays in the cytoplasm. This is demonstrated in the images presented in Figure 4. The results suggested that it does not make a difference as to whether the cells are fixed and then aspirated or aspirated and then fixed after the dexamethasone treatment (Figure 5). Based on these results it was concluded that the cells adhere tightly to the wells and the method used for aspiration does not create enough force to detach them from the wells. To be consistent with the original screening assay protocol it was decided to aspirate the wells and then fix the cells (9). Based on the results, it was then determined that the cells should be treated with 100nM dexamethasone in order to achieve maximal translocation of the GR-GFP to the nucleus. 100nM dexamethasone is far enough into the signal plateau that small variations in dexamethasone concentration due to error should not affect the results. These results were consistent with the published results from the original assay development and optimization manuscript (9).

Once the conditions for the GR-GFP translocation assay were determined it was necessary to show a proof of concept that inhibition of dynein by a small-molecule would in fact inhibit the translocation of the GR-GFP in this cell-based assay. Unfortunately the data showed that the published dynein inhibitors actually fluoresce in the GFP channel thereby confounding the interpretation of the data (Figures 8 & 9). Based on these data it was determined that the best course of action would be to test hsp90 and hsp70 inhibitors and microtubule perturbagens

in the GR-GFP translocation assay. Consistent with previous publications both hsp90 inhibitors, 17-AAG and STAT9090, inhibited Dex-induced GR-GFP translocation to the nucleus (9, 10). Conversely, the hsp70 inhibitor MAL3-101 did not inhibit translocation nor did the microtubule perterbagens (Figure 10).

Inhibition of hsp70 did not inhibit translocation most likely due to the fact that hsp70 is involved in earlier steps of the maturation of the GR (12). Once hsp90 is bound and opens the LBD of the GR most of the hsp70 bound to the complex detaches (11). For an hsp70 inhibitor to inhibit GR translocation the inhibitor would need to be added to the cells at the same time that the tetracycline is removed. The 3617.4 cell line utilizes a tet-off system to suppress GR-GFP transcription. Inhibition of hsp70 at that point would be expected to hinder GR maturation and import of hsp90 to the complex. This experiment should be performed in future studies.

3.0 CHARACTERIZATION OF HIT COMPOUNDS

3.1 INTRODUCTION

From the original HCS in the GR translocation assay, 112 hit compounds with IC50s of ≤ 10μM (chosen because 10μM was determined to be a good potency cut off for the following analyses) were found to inhibit GR translocation from a library of approximately 220,000 compounds. To reduce the number of hit compounds to be further tested for their ability to selectively inhibit hsp90, the compounds were analyzed for: their biological promiscuity using PubChem; a PAINS (25) search database created by Dr. Xiangqun Xie's laboratory at the University of Pittsburgh;, drug-like properties in a medicinal chemistry analysis using Instant JChem from Chem Axon; and a small-molecule docking simulation using the SYBYL software from Certara.

PubChem is a database created and updated by the National Institutes of Health (NIH) that allows users to perform queries to bring back compound information including physical properties and activity in biological assays (24). The PAINS search database allows users to search for possible assay interferences and promiscuity of the compound based on structures and functional groups known to interact with non-specific proteins (25). SYBYL is software that utilizes protein data bank (PDB) files of x-ray crystal structures of proteins to allow the user to identify binding pockets on the protein and simulate binding of compounds (27). The user can

set the simulation to identify a pocket on the crystal structure of the protein as the binding site to be tested against a compound library. The algorithm in SYBYL will search for possible interactions between the binding pocket and each compound. This generates a docking score that helps the user predict the likelihood that a given compound will bind the programmed binding pocket on the protein being analyzed. A medicinal chemistry analysis was done in order to evaluate the drug-like properties of the compounds. By inputting the simplified molecular-input-line-entry system (SMILES) structure of compounds into the Instant JChem this generates values for the LogP, Total polar surface area, hydrogen-bond acceptor, hydrogen-bond donor, rotatable bonds, lead likeness, Lipinski Rule of 5 (pass or fail) Rule of 3 (pass or fail), Veber Filter (pass or fail), and Muegge filter (pass or fail). This aids in determining whether a compound is a good candidate for further drug development.

The Log P, total polar surface area, hydrogen-bond acceptors, hydrogen-bond donors, rotatable bond, lead likeness, and the Lipinski Rule of 5 were all used under their basic definitions (37, 38). The Rule of 3 is a set of rules for lead-like compounds that may be fragments that can be expanded upon during the lead optimization process and includes: molecular weight $\geq$ 300, Clog P (LogP based on structure) $\leq$ 3, rotatable bonds $\leq$ 3, hydrogen-bond donors $\leq$ 3, hydrogen-bond acceptors $\leq$ 3, and polar surface area $\leq$ 60 angstroms squared(38). The Veber Rule determines good bioavailability in rats and is based on molecular flexibility, polar surface area, and hydrogen bonding (38). The Veber Rule identifies compounds with rotatable bonds $\leq$ 10 and polar surface area $\leq$ 140 angstroms squared or total hydrogen bonds (acceptors plus donors) $\leq$ 12 (38). The Muegge filter identifies compounds that have molecular weight < 500, CLogP < 5, and a polar surface area < 120 angstroms squared and only includes compounds that contain C, N, O, S, H, P, Cl, Br, F, I, Na, K, Mg, Ca, and Li (41). This

filter also identifies compounds that have combinations of two pharmacophore points which are functional groups that include: amine, amide, alcohol, ketone, sulfone, sulfonamide, carboxylic acid, carbamate, guanidine, amidine, urea, and ester. Lastly, compounds that contain structures with know toxicities are removed (41).

3.2 SPECIFIC AIM

The goal of these simulations was to evaluate whether any of the GR-GFP translocation inhibitor hits might be hsp90 inhibitors.

3.3 METHODS

Pubchem Search

The substance identification numbers (PubChem SIDs) of hit compounds with IC50s of 10μM or less were entered into the PubChem query. The number of active, inactive, inconclusive, unspecified, and total flags (total number of bioassays each compound was tested in) were extracted from the "biological test results" section. The number of active flags (bioassays in which the compound was designated active) was divided by the total number of bioassays the substance has been tested in to give the percent active flags. Compounds were categorized by < 5%, 5-8%, 10-15%, and greater than 15% active flags. Active flags is described as the number of targets that the compound was found to have activity against in a biological assay.

PAINS Search

Compound SMILES were collected from the PubChem website. The SMILES were entered into the search window on the PAINS website from the Xie lab. The database would then output whether the compound was a PAINS compound or not (25). This model compares the structures of the compounds to known compound structures that have been found to be PAINS compounds.

Medicinal Chemistry Analysis

Instant JChem was set to give outputs for LogP, Total polar surface area, hydrogen-bond acceptor, hydrogen-bond donor, rotatable bonds, lead likeness, Lipinski Rule of 5, Rule of 3, Veber Filter, and Muegge filter. SMILES were entered into Instant JChem and the software then calculated the values for all parameters. Once these values were acquired the structures of the compounds were analyzed to remove those compounds that were highly reactive and/or possibly toxic. Once all these results were combined, compounds that best fit the set criteria described above were picked to be further analyzed.

SYBYL Docking Simulation

The PDB file 1A4H (a co-crystal structure of yeast hsp90 and geldanamycin) was acquired from the RCSB Protein Data Bank (www.rcsb.org). Water was removed from the file and hydrogens were added to the structure. Geldanamycin was removed from the crystal structure and the pocket were geldanamycin was bound was identified as the binding pocket, which is the ATP binding site. A SMILE (.smi) file was created using the SMILES from the hit compounds. This file was then loaded as the ligand source and the docking simulation was run in the Surflex-Dock Screen docking mode.

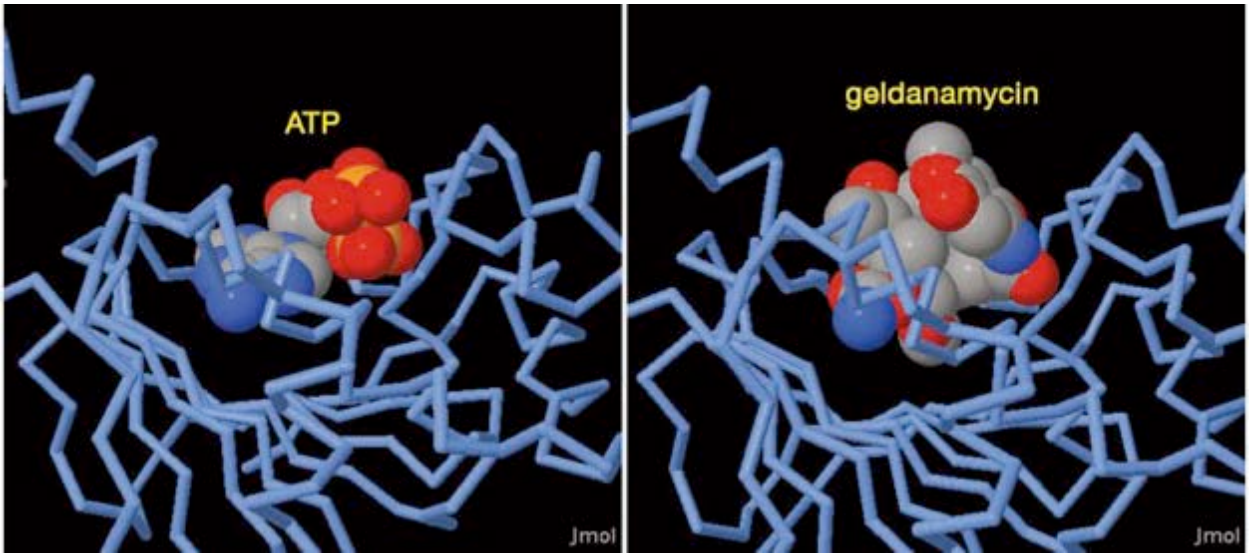

Figure 11: ATP and Geldanamycin Binding Hsp90
Geldanamycin is a natural product from Steproyces bacteria. It was the first reported inhibitor of hsp90. Geldanamycin binds the ATP-binding site of hsp90, thus blocking the binding of ATP and inhibiting the conformational changes needed for hsp90's chaperone function. The right image is from the PDB 1yet, the left image is from PDB 1am1. This binding site was used in the SYBYL docking simulation described in this thesis as the binding pocket to generate binding scores if the hit compound list. Image acquired from pdb.org Molecule of the Month and duplicated freely under the CC-BY-3.0 license (42)

3.4 RESULTS

65 compounds, from the original 112, with active flags of 0-10% (Table 1) were further analyzed for PAINS, medicinal chemistry properties, and SYBYL docking of hsp90. Seven were found to be possible PAINS compounds; indicated with (*) in Table 1. The most common targets that were identified for the compounds were the dopamine receptor D2 (DRD2), tissue-nonspecific alkaline phosphatase (ALPL), induced myeloid leukemia cell differentiation protein (MCL1), acid alpha-glucosidase (GAA), and peroxisome proliferator-activated receptor gamma (PPARG).

Pubchem SID	GR-GFP HCS IC50 uM	Total Flags	% Active Flags	Targets
26725277*	9.4	561	2.1	Trpc6,VDR,NFE2L2,DRD2,Trpc4
14729341	1.5	670	2.5	DRD2, ALPL, GAA, MCL1, MPI
24810875	6.2	605	2.8	MCL1,GAA,ALPL,PPARG,DRD2
26725379	9.7	550	2.9	CHRM5,CHRM4,CHRM1,RGS4,DRD2
24835144	6.0	504	3.0	MPI,GAA,ALPL,PPARG,DRD2
26659974	3.7	568	3.0	DRD2, RGS4, CHRM1, CHRM4, CHRM5
24812564	3.8	513	3.1	DRD2, ALPL, GAA, MPI, PPARG
24832777	10.0	532	3.2	RGS4,MPI,ALPL,PPARG,DRD2
24836477	4.5	495	3.2	DRD2, PPARG, ALPL, GAA, MPI
26659438	7.3	569	3.3	CHRM4,CHRM1,CFTR,RGS4,DRD2
26731745	9.0	478	3.3	CHRM4,CHRM1,TIM10,RGS4,DRD2
26663384	5.9	562	3.4	RGS4,CFTR,SLC5A7,NFE2L2,DRD2
24837780	7.8	638	3.6	GAA,CFTR,ALPL,PPARG,DRD2
24808613	8.6	459	3.9	MPI,ALPL,PPARG,DRD2,TNFRSF10B
14731316	8.6	685	4.2	MPI,MCL1,GAA,ALPL,DRD2
24793559	8.2	631	4.3	MCL1,GAA,ALPL,PPARG,DRD2
24808536	6.8	551	4.4	CFTR,ALPL,Hsf1,PPARG,DRD2
24831419	8.5	637	4.7	MC4R,GAA,ALPL,PPARG,DRD2
24708194	2.8	603	4.8	DRD2, ALPL, GAA, MCL1, MPI
17508477	3.9	672	5.1	MRGPRX1, DRD2, SLC5A7, ALPL, GAA
26664573	7.4	573	5.2	CHRM1,NLRP3,RGS4,CFTR,DRD2
24821616	7.2	540	5.4	MPI,DRD2,ALPL,PPARG,MITF
24789826	8.9	640	5.5	MCL1,GAA,ALPL,DRD2,MITF
14732770*	2.0	698	5.6	RGS4, MRGPRX1, ALPL, CFTR, DRD2
24785468	9.5	643	5.6	GAA,ALPL,PPARG,DRD2,RGS4
26725810	4.7	569	5.6	DRD2, RGS4, CFTR, CHRM1, CHRM4
17510018*	8.3	547	5.9	ALPL,NFE2L2,PPARG,DRD2,MITF
24830204	9.3	647	6.5	ALPL,PPARG,DRD2,MRGPRX1,MITF
22406089	6.9	661	6.5	TP53,GALR2,DRD2,CFTR,MITF
24827565	4.0	641	6.6	ALPL, CFTR, GAA, MCL1, MPI
24811325	4.2	625	6.6	TNFRSF10B, DRD2, ALPL, GAA, MPI
17513591	4.2	639	6.7	MRGPRX1, DRD2, ALPL, CFTR, GAA
17504722	7.8	664	6.8	MPI,GAA,ALPL,MCL1,CFTR
17514011	0.6	515	7.0	DRD2, Trpc4, ALPL, GAA, KCNQ1
22409186	9.0	510	7.1	MCL1,GAA,ALPL,PPARG,DRD2
24820374	1.6	376	7.2	PPARG, ALPL, GAA, MCL1, MPI
24821031	0.9	583	7.4	GNAO1, PPARG, ALPL, MPI, MAP4K2
17387987	5.4	702	7.4	DRD2, JAK2, TIM10, ALPL, GAA
24817684	7.4	554	7.6	MPI,GAA,ALPL,DRD2,MITF
17413916	8.6	691	7.7	GAA,ALPL,VDR,DRD2,RGS4

14739918	6.6	704	7.8	GAA,ALPL,Kcnq2,KCNQ1,DRD2
22408535	6.6	665	7.8	MCL1,GAA,ALPL,SLC5A7,DRD2
22403487	8.0	651	8.0	ALPL,PSIP1,MCL1,DRD2,MITF
24830158	8.9	571	8.4	ALPL,PPARG,Kcnq2,KCNQ1,DRD2
17509721	9.7	593	8.4	MCL1,GAA,ALPL,DRD2,TNFRSF10B
24812054	9.6	592	8.4	MCL1,GAA,ALPL,PPARG,DRD2
24818889	4.6	561	8.6	MITF, DRD2, Hsf1, ALPL, GAA
24819034	8.6	647	8.7	ALPL,ADRB2,KCNQ1,IDH1,DRD2
14743736	9.2	707	8.9	MCL1,GAA,ALPL,DRD2,MRGPRX1
24826599*	9.5	670	9.0	KCNQ1,FXN,HKDC1,DRD2,MITF
24803246	8.4	566	9.0	MPI,GAA,ALPL,DRD2,TNFRSF10B
22408394	6.6	655	9.2	GAA,ALPL,PPARG,DRD2,MITF
17517377	6.8	683	9.2	GAA,ALPL,DRD2,MITF,TNFRSF10B
24841212	9.0	579	9.3	GAA,ALPL,DRD2,MITF,TNFRSF10B
17412468	5.0	686	9.3	DRD2, MCL1, ALPL, GAA, MPI
14743646	9.4	711	9.4	MCL1,GAA,ALPL,DRD2,RGS4
17402075	1.5	711	9.6	MRGPRX1, DRD2, MCL1, ALPL, GAA
17387926*	3.8	657	9.6	DRD2, ALPL, GAA, MCL1, MPI
24809046	8.0	465	9.7	RGS4,PPARG,MPI,ALPL,DRD2
24809046	8.0	465	9.7	RGS4, MPI,ALPL,PPARG
22404816	3.0	587	9.7	CXCR6, ALPL, DRD2, GAA, MPI
26725671*	7.0	582	9.8	CHRM1,TIM10,Alpi,DRD2,RGS4
849046	1.5	826	9.9	Trpc4, ALPL, DRD2, SLC5A7, RGS4
24785301	8.8	573	9.9	MPI,GAA,DRD2,ALPL,Kcnq2
17403527*	0.6	472	10.0	GNAO1, MAP4K2, ALPL, GAA, MCL1

TABLE 1: 65 compounds from PubChem search that were found to have 0-10% active flags.
Compounds are identified by their substance identification number (SID). The number of flags refers to the number of reported active designations in biological assays. (*) compounds are compounds that were found to be PAINS in the PAINS database search.

The 65 compounds from the PubChem search were analyzed for drug-like and lead-like properties in a medicinal chemistry analysis using Instant JChem and then further analyzed for reactivity, possible toxicity, and ease of synthesis, which are important for drug development. The results from the analysis are shown in Table 2. Based on the SMILES of each compound,

Instant JChem produced values for LogP, total polar surface area, hydrogen-bond acceptor, hydrogen-bond donor, rotatable bonds, lead likeness, Lipinski Rule of 5, Rule of 3, Veber Filter, and Muegge filter. Acceptable LogP values were 1-5 with 1-4 being preferred. Compounds with LogP values in this range are good drug-like candidates because they are likely to be orally absorbed and distributed through the blood stream. They will be hydrophobic enough to partition into the lipid bilayer, but not so hydrophobic that they stay in the lipid bilayer. Total polar surface area values of 120-122 angstroms squared were acceptable, however values below 120 angstroms squared were preferred. Hydrogen-bond acceptors of 0-10 were considered acceptable with 1-6 being preferred. Hydrogen-bond donors of 0-5 were considered acceptable with 1-5 being preferred. Compounds having 0-10 rotatable bonds were considered acceptable with 0-8 being preferred. Meeting three of the four Lipinski Rule of 5 was a pass whereas the Veber filter, Muegge filter, and the Rule of 3 where a pass if all parameters were met and a fail if a single parameter was not met. A majority of drugs that have made it to the market possess these properties (37-41).

Results	Formula	SID	MW	LogP	TPSA	HBA	HBD	RB	Lead likeness	Lipinski rule of 5 (3 of 4)	Veber filter	Rule of 3	Muegge filter
NO2 flag No H bond donors yet potent	C12H10 BrN3O3	14729341	324.13	2.44	78.03	4	0	4	TRUE	TRUE	TRUE	FALSE	TRUE
NO2 flag No H bond donors yet potent	C12H9 BrN4O5	24810875	369.13	2.38	121.2	6	0	5	TRUE	TRUE	TRUE	FALSE	TRUE
NO2 flag No H bond donors yet potent	C13H12 BrN3O4	26659974	354.16	2.28	87.26	5	0	5	TRUE	TRUE	TRUE	FALSE	TRUE

NO2 flag No H bond donors yet potent	C12H9BrFN3O3	24812564	342.12	2.58	78.03	4	0	4	TRUE	TRUE	TRUE	FALSE	TRUE
NO2 flag No H bond donors yet potent	C11H10BrN3O2	26663384	296.12	2.93	60.96	3	0	3	TRUE	TRUE	TRUE	FALSE	TRUE
NO2 flag No H bond donors yet potent	C12H9Br2N3O3	14731316	403.03	3.21	78.03	4	0	4	TRUE	TRUE	TRUE	FALSE	TRUE
NO2 flag	C10H13N5O4	26725810	267.24	1.10	110.4	5	1	3	TRUE	TRUE	TRUE	FALSE	TRUE
NO2 flag	C14H17N3O4S	17387987	323.38	3.36	95.1	5	0	6	TRUE	TRUE	TRUE	FALSE	TRUE
NO2 flag No H bond donors yet potent	C10H8ClN3O4S	22404816	301.71	2.26	95.1	5	0	3	TRUE	TRUE	TRUE	FALSE	TRUE
a-halo amide	C13H16ClNO	24835144	237.73	2.67	20.31	1	0	2	TRUE	TRUE	TRUE	TRUE	TRUE
a-halo ketone	C11H11ClN2O2	24832777	238.67	1.69	48.03	2	0	3	TRUE	TRUE	TRUE	TRUE	TRUE
a-halo amide	C16H23ClN2O	24836477	294.82	2.77	23.55	2	0	4	TRUE	TRUE	TRUE	FALSE	TRUE
a-halo amide	C12H16ClNO2	24837780	241.71	1.88	29.54	2	0	5	TRUE	TRUE	TRUE	FALSE	TRUE
a-halo amide	C12H13ClFNO	24808613	241.69	2.66	20.31	1	0	1	TRUE	TRUE	TRUE	TRUE	TRUE

a-halo ketone	C12H13 ClN2O2	24830204	252.70	1.71	48.03	2	0	3	TRUE	TRUE	TRUE	TRUE	TRUE
a-halo amide	C8H9Cl2 NOS	24827565	238.13	2.36	20.31	1	0	3	TRUE	TRUE	TRUE	TRUE	TRUE
a-haloamide	C21H23 ClFN3O2	17509721	403.88	3.17	62.3	3	1	6	TRUE	TRUE	TRUE	FALSE	TRUE
a-halo ketone	C13H11C lFN3O	24819034	279.70	2.04	53.49	4	2	5	TRUE	TRUE	TRUE	FALSE	TRUE
a-halo amide remove	C17H14 ClN3O	14743736	311.77	3.96	46.92	2	1	4	TRUE	TRUE	TRUE	FALSE	TRUE
a-halo ketone	C15H16 ClNO2	24826599	277.75	2.24	31.23	2	0	4	TRUE	TRUE	TRUE	FALSE	TRUE
a-halo amide remove	C15H12 Cl2N2O3	24803246	339.17	3.88	63.45	3	0	5	TRUE	TRUE	TRUE	FALSE	TRUE
a-halo amide remove	C14H13 ClN2O2S	17517377	308.78	2.61	45.81	2	0	3	TRUE	TRUE	TRUE	FALSE	TRUE
fragment /No H-Bonds/ possible reactive nucleous	C10H12C l2N2 O2	24821616	263.12	2.60	49.74	3	0	3	TRUE	TRUE	TRUE	TRUE	TRUE
fragment /No H-Bonds/ possible reactive nucleous	C11H7Cl 2FN2O	24789826	273.09	2.86	32.67	2	0	2	TRUE	TRUE	TRUE	TRUE	TRUE
possible reactive nucleous flag	C17H18C l2N4O3	22406089	397.26	1.98	82.08	4	1	6	TRUE	TRUE	TRUE	FALSE	TRUE

fragment /No H-Bonds/ possible reactive nucleous	C13H12Cl2N2O	22409186	283.15	3.74	32.67	2	0	2	TRUE	TRUE	TRUE	FALSE	TRUE
No-H bond donors/ fragment /possible reactive nucleous	C10H12Br2N2O2	24817684	352.02	2.93	49.74	3	0	3	TRUE	TRUE	TRUE	FALSE	TRUE
possible reactive nucleous flag	C14H12Cl2F3N3O2	22408535	382.17	2.88	54.67	3	0	5	TRUE	TRUE	TRUE	FALSE	TRUE
possible reactive nucleous flag	C15H15Cl2N3O2	22403487	340.21	2.66	54.67	3	0	5	TRUE	TRUE	TRUE	FALSE	TRUE
Aliphatic ketone flag/ fragment /no H-bonds, posibble reactive nucleous flag	C7H6Br2N2O2	24818889	309.94	1.13	49.74	3	0	2	TRUE	TRUE	TRUE	FALSE	TRUE
possible reactive nucleous flag	C16H16Cl2N4O3	22408394	383.23	1.54	82.08	4	1	5	TRUE	TRUE	TRUE	FALSE	TRUE
possible reactive nucleous flag	C14H10Cl2N4O3	24841212	353.16	0.71	82.08	4	1	2	TRUE	TRUE	TRUE	FALSE	TRUE
ab conjugated cyano possible flag, high logP	C21H16ClN3OS	17513591	393.89	5.62	65.78	3	1	4	FALSE	TRUE	TRUE	FALSE	FALSE
ab conjkugated cyano, possible flag, high logP	C21H15Cl2N3OS	17514011	428.33	6.22	65.78	3	1	4	FALSE	TRUE	TRUE	FALSE	FALSE
Posible reactive nucleous, High logP	C18H13BrN4S	17412468	397.29	5.00	61.6	4	1	4	FALSE	TRUE	TRUE	FALSE	TRUE

OK	C24H22N2O	17387926	354.44	4.82	59.04	3	1	2	FALSE	TRUE	TRUE	FALSE	TRUE
Not sure Maybe OK	C24H21ClN2O5	24820374	452.89	4.40	93.73	4	2	7	FALSE	TRUE	TRUE	FALSE	TRUE
Not sure Maybe OK	C28H22N2O6	24821031	482.48	4.27	102.96	4	2	9	FALSE	TRUE	TRUE	FALSE	TRUE
fragment	C7H5NOS	24830158	151.19	1.36	29.1	1	1	0	TRUE	TRUE	TRUE	TRUE	FALSE
fragment	C7H4FNOS	24785301	169.18	1.50	29.1	1	1	0	TRUE	TRUE	TRUE	TRUE	FALSE
ab-conjugated	C19H20O4	26725277	312.36	3.51	63.6	4	1	4	TRUE	TRUE	TRUE	FALSE	TRUE
vinilogous amide maybe issue	C17H14BrClN2O	14732770	377.66	4.70	41.13	3	2	3	FALSE	TRUE	TRUE	FALSE	TRUE
ab conjugated remove	C18H17NO2	24785468	279.33	4.00	46.17	2	1	4	FALSE	TRUE	TRUE	FALSE	TRUE
curcumin type remove	C20H21N3O	17510018	319.40	2.62	46.09	4	0	3	TRUE	TRUE	TRUE	FALSE	TRUE
maybe OK	C17H13NO3	24811325	279.29	3.03	47.89	3	0	3	TRUE	TRUE	TRUE	FALSE	TRUE
ab conjugated remove	C20H30O5	17504722	350.45	0.50	97.99	5	4	0	TRUE	TRUE	TRUE	FALSE	TRUE

a,b conjugated nitro, high NRB	C16H19NO8	17413916	353.32	1.78	114.2	6	0	12	FALSE	TRUE	FALSE	FALSE	TRUE
no H-bonds High NRB	C15H25NO7	14739918	331.36	0.62	91.37	5	0	11	FALSE	TRUE	FALSE	FALSE	TRUE
No H-bonds flag,	C9H6ClN5	24812054	219.63	2.33	55.97	4	0	0	TRUE	TRUE	TRUE	FALSE	TRUE
redox	C22H18N2O4S	14743646	406.45	2.82	76.66	6	2	5	TRUE	TRUE	TRUE	FALSE	TRUE
OK	C16H10F3N5OS3	17402075	441.47	4.31	93.79	5	2	4	TRUE	TRUE	TRUE	FALSE	TRUE
MW too high/redox fag	C31H27N3O6	26725379	537.56	4.13	107.92	8	0	9	FALSE	TRUE	TRUE	FALSE	TRUE
NO2 flag No H bond donors yet potent	C12H8N6O2S	24809046	300.30	3.20	99.63	6	0	4	TRUE	TRUE	TRUE	FALSE	TRUE
Same as compound above, NO2 flag, No H bond donors yet potent	C12H8N6O2S	24809046	300.30	3.20	99.63	6	0	4	TRUE	TRUE	TRUE	FALSE	TRUE
redox	C16H11N3O6S	26725671	373.34	2.53	118.85	6	1	4	TRUE	TRUE	TRUE	FALSE	TRUE
too simple, LogP high highly lipophilic	C14H22O2	849046	222.32	5.06	40.46	2	2	6	FALSE	TRUE	TRUE	FALSE	FALSE

Highly conjugated positively charged	C21H21IN2OS	17403527	476.37	0.04	24.19	1	0	5	FALSE	TRUE	TRUE	FALSE	TRUE
NO2 flag No H bond donors yet potent	C15H20O4	26731745	264.32	2.50	44.76	4	0	9	TRUE	TRUE	TRUE	FALSE	TRUE
ab conjugated remove	C18H16ClNO5S	24793559	393.84	5.25	92.7	4	2	7	TRUE	TRUE	TRUE	FALSE	FALSE
alkyl-halide	C15H19ClO4S	24808536	330.83	3.40	52.6	2	0	10	TRUE	TRUE	TRUE	FALSE	TRUE
OK	C18H26N4O4	24831419	362.42	1.96	93.65	6	1	8	TRUE	TRUE	TRUE	FALSE	TRUE
maybe OK but not a lead MW high	C28H28N2O6	24708194	488.53	2.76	101.06	5	0	8	FALSE	TRUE	TRUE	FALSE	TRUE
OK but not lead like	C21H17N3OS	17508477	359.44	4.84	59.22	3	1	1	FALSE	TRUE	TRUE	FALSE	TRUE
ab conjugated remove	C12H11NO6	26664573	265.22	2.42	95.74	4	0	6	TRUE	TRUE	TRUE	FALSE	TRUE
		26659438	0		0	0	0	0	FALSE	TRUE	TRUE	FALSE	FALSE

Table 2: Results from Med Chem Analysis using Instant Jchem.
Parameters were set in Instant JChem to determine drug-likeness and Lead-likeness. Other considerations were functional groups and reactivity. Green indicates that the parameter passed the criteria, Yellow indicates that the parameter value is mostly passed, and Red indicates that the parameter failed the criteria.

CID	Total_Score	Notes
24708194	7.57	
24821031	7.33	
849046	6.99	
17510018	6.49	PAINS
26731745	6.07	
22406089	5.84	
24793559	5.82	
24808536	5.79	
14743646	5.76	
24820374	5.67	
22408394	5.62	
24785468	5.57	
24819034	5.53	
17403527	5.53	
26725379	5.52	
24831419	5.40	Ok Med Chem Analysis
24837780	5.37	
17413916	5.36	
24831419	5.23	
14732770	5.22	
17514011	5.20	
17387987	5.12	
14739918	5.08	
17513591	4.98	
26725671	4.94	
24830204	4.84	
26659974	4.80	
26664573	4.80	
24826599	4.66	
24812564	4.64	
22408535	4.53	
24841212	4.45	
24803246	4.40	
22404816	4.37	
26663384	4.36	

22403487	4.33	
24785301	4.18	
24810875	4.18	
24811325	4.17	
26725810	4.17	
24836477	4.14	
24835144	4.14	
17412468	4.06	
17509721	4.00	
14731316	3.81	
22409186	3.70	
24817684	3.55	
17387926	3.50	
24832777	3.28	
24809046	3.22	
24809046	3.22	
24830158	3.21	
24821616	3.19	
17504722	3.11	
17517377	3.09	
24789826	3.06	
24818889	3.00	
17508477	2.94	
24808613	2.84	
14743736	2.68	
17402075	2.52	Ok Med Chem Analysis
24827565	2.13	
24812054	1.55	

Table 3: Docking Scores from SYBYL Docking Simulation.
The 5 compounds highlighted in yellow have a high likelihood of binding yeast hsp90 at the geldanamycin binding site. Compounds highlighted in green were found to have favorable drug-like properties in the medicinal chemistry analysis.

Selected hit compounds from the PubChem analysis were docked against the geldanamycin binding site, results can be found in Table 3. Compounds with a score of 6 or greater (based on the parameters created by the Xie lab, School of Pharmacy, University of Pittsburgh, in this SYBYL docking simulation) were determined to have a high probability of

binding yeast hsp90 at the geldanamycin binding site, these compounds are highlighted in yellow (a score of 6 means μM binding). One of these compounds, 17510018, was found to be a PAINS compound. Compounds that were found to have favorable drug-like properties in the medicinal chemistry analysis are noted in Table 3.

3.5 DISCUSSION

The result of these analyses and simulations was the prioritization of five compounds for further investigation (Table 4). For the purpose of this study when identifying a small-molecule inhibitor of a protein it is also important that the small-molecule is selective for the protein target. A compound that is not selective for a protein target has the potential to produce negative side effects in a clinical setting. The PubChem search, coupled with the PAINS database search, identified hit compounds that have low promiscuity, i.e. compounds that are not a PAINS compound and have less than 8% active flags.

Once compounds with low promiscuity were identified it was necessary to predict whether a given compound would bind hsp90. Compounds with SYBYL docking scores of six or greater using this docking model have an increased probability of binding hsp90. It is also important to take into consideration whether the compound is drug-like, i.e. has acceptable pharmacokinetic properties.

Table 4 shows the results of each test for the five compounds selected from the original 112 hit compounds with translocation IC50s < 10 μM. The first two compounds were chosen based on their SYBYL docking score ratings being 1 and 2, respectively, indicating a higher probability of binding hsp90 in the geldanamycin binding pocket when compared to the rest of

the 65 hit compounds, narrowed down from the 112 hit compounds. These compounds also appear to have low promiscuity, based on the PubChem search, they have 4.8% and 7% active flags, respectively, and were not PAINS compounds. In the medicinal chemistry analysis both compounds passed most of the test criteria. Both compounds have molecular weights approaching 500, the maximum molecular weight for a drug-like compound according to the Lipinski rule of 5. This leaves little room for lead optimization if functional groups are added. Although a disadvantage compound 24708194 is the lack of hydrogen-bond donors, hydrogen bond donors can be added and the compound still has five hydrogen bond acceptors. Compound 24821031 has excellent hydrogen bonding capabilities with four hydrogen-bond acceptors and two hydrogen-bond donors. A drawback for compound 24821031 is its LogP value of 4.27, a moderately high value indicating poor aqueous solubility. Additionally the number of rotatable bonds is moderately high at nine. Overall these two compounds are good candidates due to high docking scores and for the most part have ideal drug-like properties. Two other compounds, 17402075 and 24831419, were selected as both passed all of the parameters in the medicinal chemistry analysis. They both show low promiscuity through the PubChem search and were not found to be PAINS compounds. The fifth compound was selected even though it was found to be a possible PAINS compound, however the PubChem search only came up with 1.3% active flags. This compound could possibly give some insight into which method is more reliable to determine promiscuity, the PAINS database or the PubChem search.

SID	Med Chem Analysis	SYBYL Rank	SYBYL Docking Score	Active Flags PubChem (%)
24708194	Maybe OK	1	7.5679	4.8
24821031	Maybe OK	2	7.3259	7
17402075	OK	61	2.5208	2.2
24831419	OK	16	5.3972	0.0015
17387926	Possible PAINS	48	3.4962	1.3

TABLE 4: The 5 hit compounds selected to be further characterized as hsp90 inhibitors

SID = Substance Identification Number

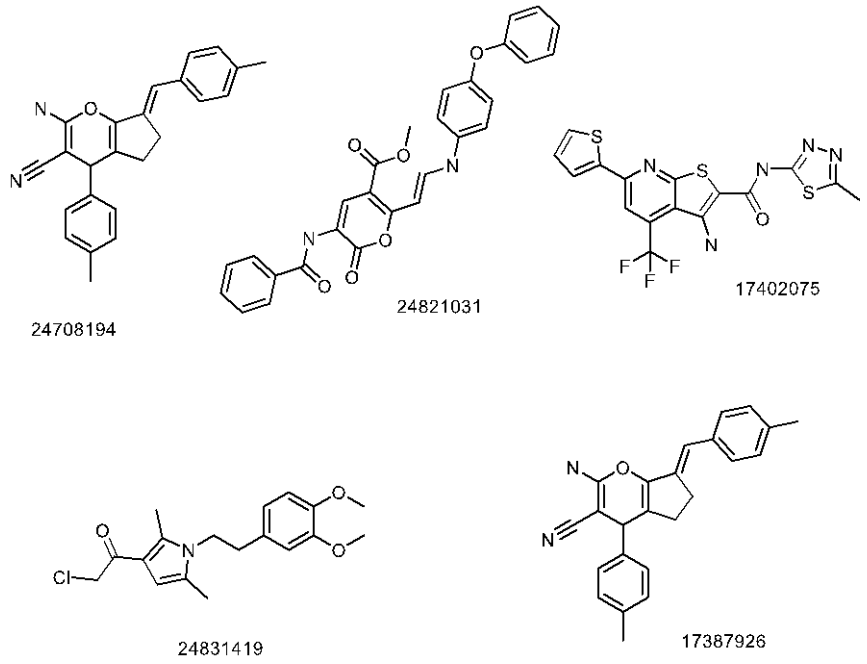

Figure 12: Structures of Selected Hit Compounds

4.0 ATPASE ACTIVITY ASSAY

4.1 INTRODUCTION

The original HCS, which involved the translocation of the GR, and the subsequent cheminformatics analysis has identified hit compounds that might be inhibitors of the ATPase activity of hsp90. To test these compounds the PiPer assay from Invitrogen, which is an enzyme coupled amplex red assay, was used to detect ATPase activity of recombinant yeast hsp90. The PiPer^{TM} assay is an enzyme-coupled assay that measures inorganic phosphate production by an ATPase (as well as phosphate produced by phosphatases). ATPase's produce inorganic phosphate by hydrolyzing ATP. The 1st coupling enzyme Maltose phosphorylase catalyzes the phosphorylation of maltose to produce glucose 1-phosphate and glucose. The 2nd coupling enzyme Glucose oxidase then catalyzes the oxidation of glucose to D-glucono-δ-lactone and hydrogen peroxide. Horse radish peroxidase, the 3rd and final enzyme in the enzyme coupled reaction, catalyzes the reaction of hydrogen peroxide with amplex red to produce the fluorescent product resorufin (43). Although enzyme coupling increases the opportunity for compound interference, it also works to show further selectivity of compounds. To account for compound interference with the enzyme coupled assay, compounds will need to be tested in an assay where inorganic phosphate is added to the mixture with compounds and the assay mix in place of the ATPase and ATP. If a compound interferes with the assay in the presence of inorganic phosphate, it is likely that that compound is inhibiting one of the enzymes in the assay mix. Final

concentrations of DTT were less than 10μM in the reaction mix per the manufacturers recommendations to prevent interference with amplex red. In order to show a compound's selectivity for hsp90, the compounds would also need to tested against other ATPases. The ATPases chosen to test selectivity of these compounds where myosin and kinesin, both motor proteins that utilize the energy of ATP hydrolysis to transport cargoes.

4.2 SPECIFIC AIM

The goal of this work was to characterize selected hits from the original HCS using an *in vitro* biochemical assay that measures ATPase activity. The assays were optimized so that a future study could assess compounds for potency, as well as selectivity, using multiple recombinant ATPases.

4.3 METHODS

Isolation of hsc82 yeast, homolog of hsp90

Recombinant yeast hsp90 (also known as hsc82, hsp90 homolog; chosen for high activity) was purified from the yeast strain ECUpep4 (33). This yeast strain contains deletions in the chromosomal HSC82 genes and a 2μm URA3 plasmid that encodes and overexpresses HSC82 using techniques based on a protocol developed by Dr. David Toft (Mayo Clinic, Rochester, MN), modified by Dr. Brodsky lab (44). Yeast cells were grown in YPD (1% yeast extract, 2% peptone, and 2% dextrose) at 26°C to an OD_{600}(optical density at 600nm) of 0.8–1.0

(logarithmic phase). Following growth to the logarithmic phase, the cells were collected from the growth media by centrifugation for five minutes at 4,700 x g and frozen at -80°C in 50mL conical centrifuge tubes for a minimum of 24 hours. Cell pellets were re-suspended in five volumes of Buffer 1 (containing 20 mM Tris-HCl, pH 7.5, 4mM EDTA, 1 mM DTT, and protease inhibitors (1 mM PMSF, 1 μg/ml leupeptin, 0.5 μg/ml pepstatin A), and lysed by bombardment with glass beads (500 μm diameter) using a vortex at its maximum setting six times for 30 seconds with 30 second rests on ice. Cells still intact after the lysing step were pelleted by centrifugation at 2800 x g for 10 minutes at 4°C and the supernatant was collected. The intact cell pellet remaining after the supernatant was decanted was frozen at -80°C to use in future hsp90 purifications. Cell membranes were then removed from the supernatant from the previous step by centrifugation at 48,000 x g for 40 minutes at 4°C. The supernatant was collected as cleared lysate and the cell membrane pellet was discarded. Protein purification was completed using the Invitrogen AKTA FPLC system. The cleared lysate was applied to a 5mL HiTrap DEAE column from Invitrogen equilibrated in 5 column volumes of buffer 1. The column was then washed with 2 column volumes of buffer 1 and with 2 column volumes of buffer 1 containing 50 mM KCl. Bound protein was eluted with a continuous KCl gradient from 0 to 1M KCL in buffer 1. Fractions were collected and analyzed by sodium sodium dodecyl sulfate-polyacrylamide gel electrophoresis (SDS-PAGE). The factions that contained a strong band at 82kDa were pooled together and desalted on a PD-10 column. The PD-10 column was equilibrated with buffer 2 containing 20 mM Tris-HCl, pH 7.5, 50 mM KCl, 1 mM EDTA, 1 mM DTT, 10% glycerol. 2.5mL of sample was added to each PD-10 column. The sample was eluted off the column with 3.5mL of buffer 2 and collected in 1mL fractions. The dialysate was loaded onto a high performance Q-Sepharose column equilibrated in buffer 2, and the column

was washed with buffer 2 and then buffer 2 containing 50 mM KCl (flow rate1.0 ml/min) at 4°C. Bound protein was eluted with a continuous KCl gradient from 0 M to 1 M KCl. Peak hsp90-containing fractions, determined by SDS-PAGE, were pooled and dialyzed in a PD-10 column against buffer 3 containing 20 mM Tris-HCl, pH 7.5, 50 mM KCl, 0.1 mM EDTA, 1 mM DTT, 10% glyercol. The final protein concentration was determined using the Peirce 660nm protein assay kit (Fisher Scientific, Pittsburgh, PA) with BSA as the standard, and the final purity of hsp90 was estimated to be approximately 80% by visual inspection of the SDS-PAGE gels.

ATPase Activity Assay

The PiPer™ Phosphate Assay kit was purchased from Fisher Scientific, Pittsburgh, PA. Samples containing the phosphate-generating enzyme were diluted to a predetermined concentration (determined by enzyme titration) in 1X reaction buffer (either the 0.1M Tris-HCl, pH 7.5 buffer provided in the kit or a published reaction buffer for that enzyme). 20μL of the diluted enzyme (predetermined for each enzyme, discussed later in the optimization steps) was added to each well testing the enzyme in a black 384-well plate. 20μL of reaction buffer, instead of diluted enzyme, was added to the negative control wells. To start the reaction 20μL of a working solution (premixed) containing 100 μM Amplex Red reagent, 4 U/mL maltose phosphorylase, 0.4 mM maltose, 2 U/mL glucose oxidase, 0.4 U/mL HRP and an experimentally predetermined concentration of ATP (different for each enzyme) was added to each well. The plate was centrifuged for 2 minutes at 100 x g. The plate was then shaken in a microplate shaker at a low-medium setting for 1 minute, The plate was read in an M5e microplate reader at time 0 in the fluorescence setting with an excitation wavelength of 530nm and an emission detection wavelength of 590. The plate was incubated at 37°C in an incubator and measurements were taken every 30 minutes for 4 hours.

In order to determine optimal assay conditions, each enzyme was tested in an enzyme titration, a substrate titration, and with a known inhibitor. The length of time required for each enzyme to be assayed was determined during the enzyme titration step.

For the recombinant yeast hsp90 five serial dilutions (7.25µg, 3.63µg, 1.81µg, 906ng, and 453ng, of protein per well) were tested in triplicate to determine the optimal amount of recombinant yeast hsp90 to be used in the assay. Based on published results from Availa et al 2006 and previous experiments, the yeast hsp90 in the PiPer assay working mix was incubated for 60 minutes at 37°C before the first read (20). Hsp90 has a slow turnover rate of ATP hydrolysis and it takes at least 60 minutes to start to see activity in the assay. Readings were taken at 0, 90, 150, 180, 210, and 240 minutes. In order to determine the optimal substrate concentration six dilutions of ATP (1mM, 500µM, 250µM, 1µM, 500nM, and 250nM) were tested in triplicate using the optimal protein amount per well determined in the enzyme titration. The final optimization step was to determine the best control inhibitor to use in the assay. Wells containing the predetermined protein amount and substrate concentration were treated with 20µM 17-AAG and Geldanamycin. In two separate experiments hsp90 was either pretreated with inhibitor and incubated at 37°C for 30 minutes before substrate was added or treated with substrate and inhibitor at the same time.

Kinesin heavy chain motor domain purchased from Cytoskeleton Inc (KR01) was diluted in five serial dilutions, (1.4µg, 700ng, 350ng, 175ng, and 0.0875ng) to determine the optimal amount of kinesin to add to each well in the PiPer assay. The plate was incubated at 37°C and readings were made at time 0 and subsequently at 20-minute intervals. The optimal substrate concentration was determined by testing the optimal amount of protein determined in the enzyme titration with six serial dilutions of ATP, 1mM, 500µM, 250µM, 125µM, 62.5µM, and 31.25µM.

Using the optimal kinesin and ATP concentrations determined by the previous experiments, 5'-adenylylimidodiphosphate (AMP-PNP) was tested in the assay at concentrations of 1mM, 0.5mM, 0.25mM, and 0.125mM as the control inhibitor. AMP-PNP is a PAN ATPase inhibitor, used here to inhibit kinesin heavy chain domain because there are no know small-molecule inhibitors of this isoform of kinesin.

To determine the optimal amount myosin (rabbit skeletal muscle, Prozyme, MW20) to use in the PiPer assay five dilutions were tested, 200μg/mL, 100μg/mL, 50μg/mL, 25μg/mL, and 12.5μg/mL. Using the optimal protein concentration determined in the enzyme titration, the optimal substrate concentration was determined by testing myosin in the PiPer assay with six dilutions of ATP, 1mM, 250μM, 100μM, 50μM, 25μM, and 12.5μM.

4.4 RESULTS

The results of the purification of recombinant yeast hsp90 are shown in the images of the SDS-PAGE gels from the purification steps (Figure 13). The percent purity was estimated from these gels by visual estimation.

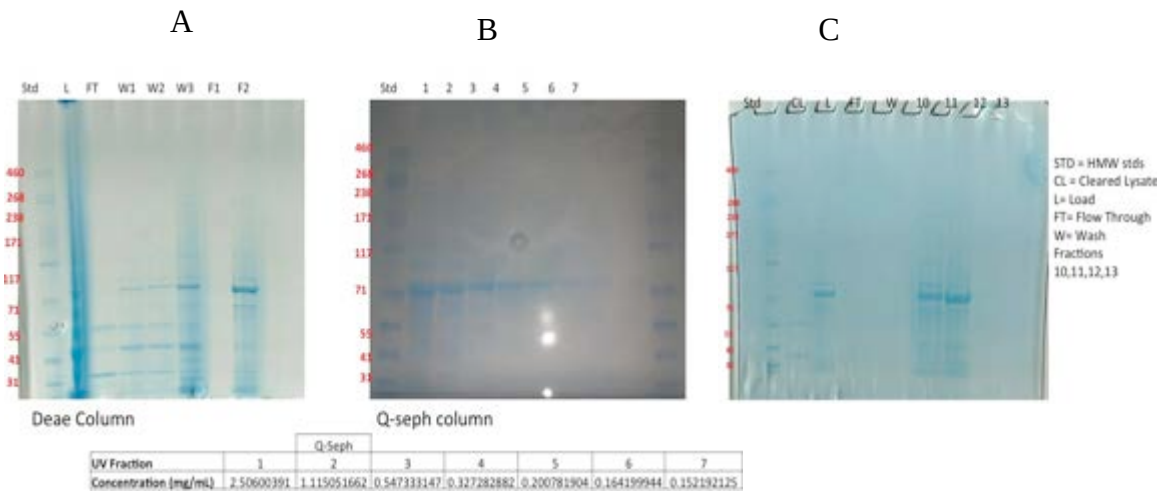

FIGURE 13: SDS-PAGE of Elution Fractions from Hsp90 Purification.
A) SDS-PAGE of Molecular Weight Standards (Std), Load (L), Flow-through (FT), Wash 1 (W1), Wash 2 (W2), Wash 3 (W3), Fraction 1 (F1), and Fraction 2 (F2) from DEAE column. B) SDS-PAGE of Molecular Weight Standards (Std), Fractions 1, 2, 3, 4, 5, 6, 7 from first Q-sepharose column. C) SDS-PAGE of Molecular Weight Standards (Std), Cleared Lysate (CL), Lysate (L), Flow-through (FT), Wash (W), and Fractions 10, 11, 12, 13 from second Q-Sepharose column.

Fraction 12 from the second Q-sepharose column from the hsp90 purification was used in the PiPer assay optimization. The optimal amount of yeast hsp90 to use was determined to be 6.25ug based on these results and the published results from Availa et al 2006 (45). The optimal time to run the assay was 240 minutes, which was the last time point, based on the signal being relatively high and approximately linear at this time point (Figure 14). The amount of substrate (ATP) to be used in the assay was determined to be 500μM ATP in a substrate titration (Figure 15A). The Km of this protein prep for ATP was estimated to be 188 μM (Figure 13 B);the published Km for yeast hsp90 is 300μM (47).

A

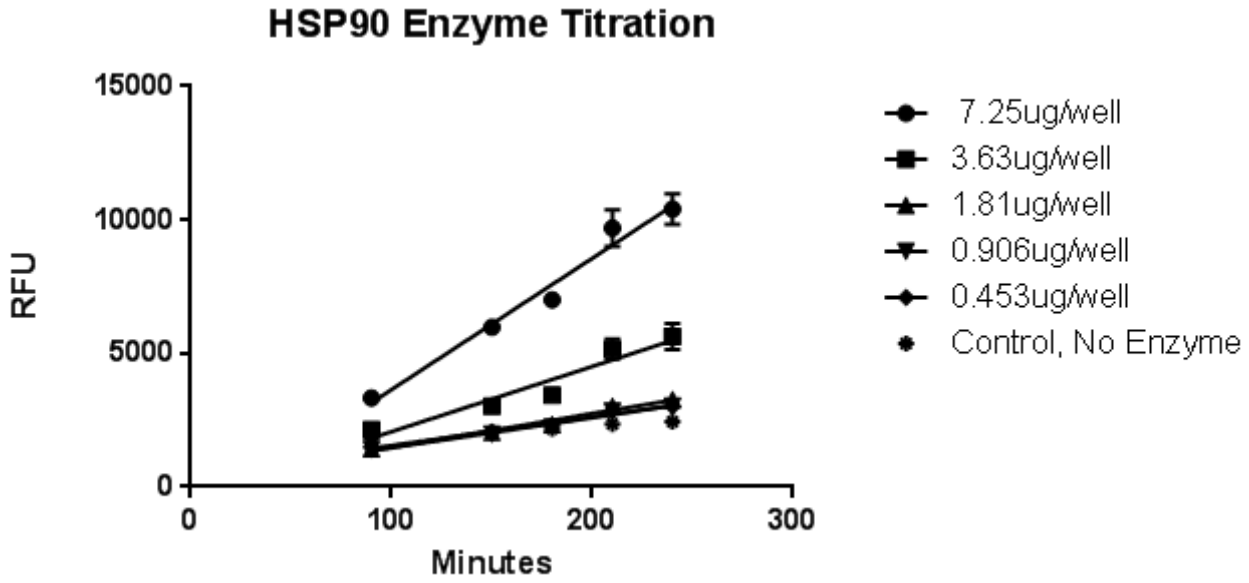

B

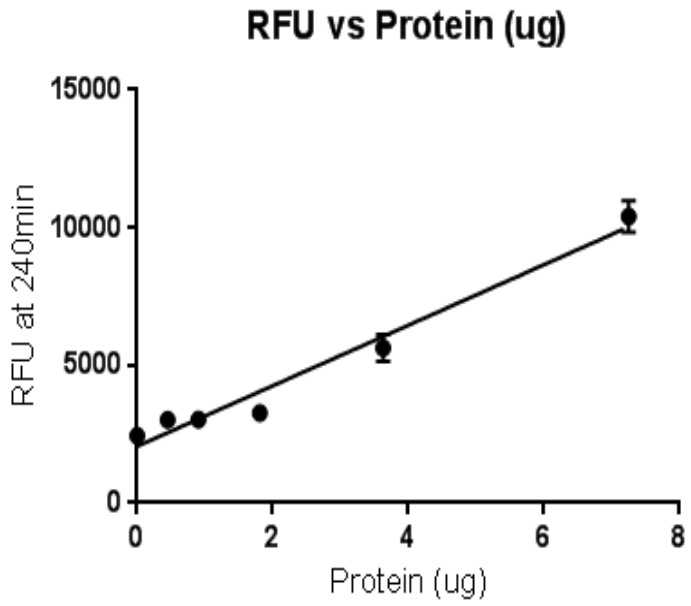

FIGURE 14: Enzyme Titration of Recombinant Yeast Hsp90.
A) Enzyme titration of hsp90 over time in minutes. Activity read in relative fluorescence units (RFU)
B) RFU vs protein amount (μg) at 240 minutes.
Three replicates. Error bars in standard deviation. Data representative of three separate experiments over three separate days.

A

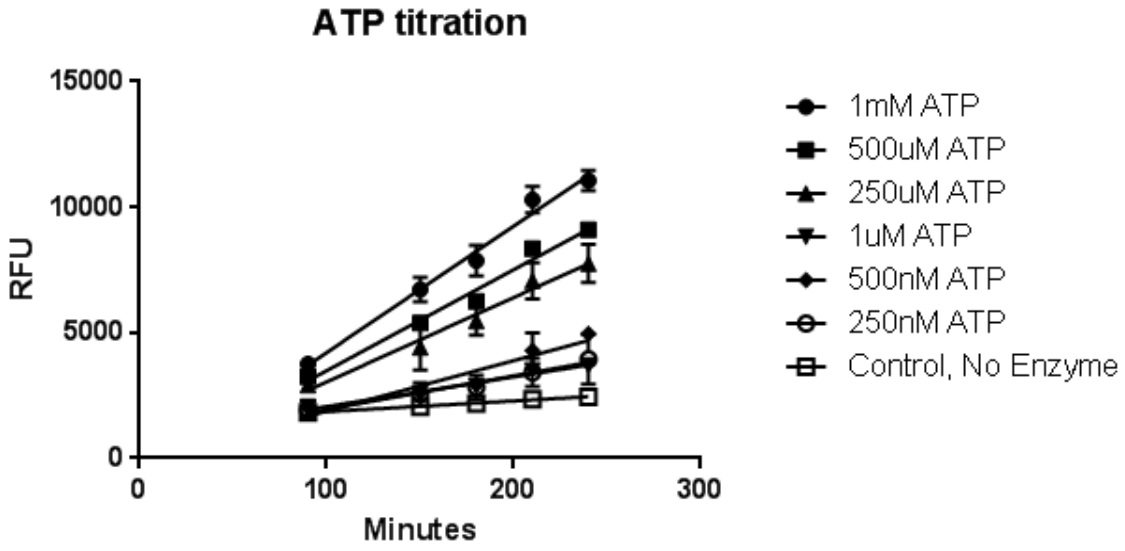

B

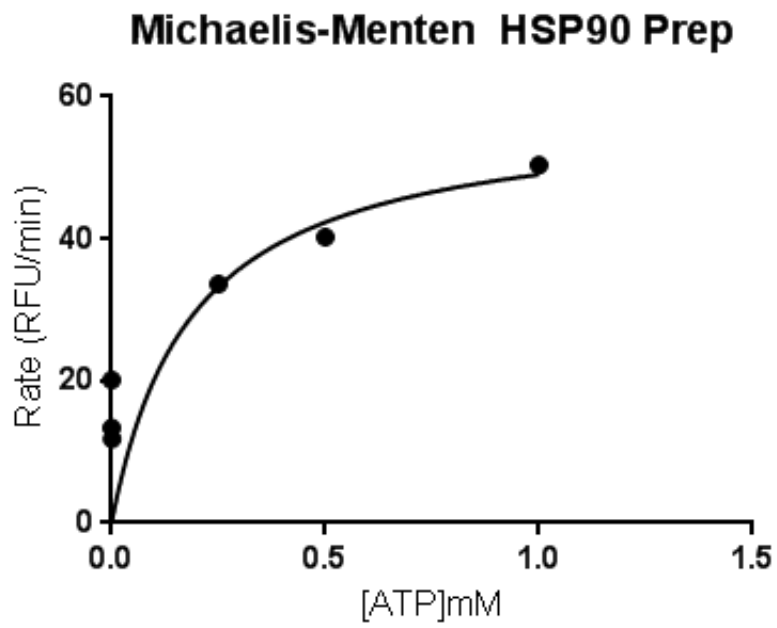

FIGURE 15: Substrate Titration of Recombinant Yeast Hsp90

A) Relative fluorescence units over time in minutes for six concentrations of ATP. Error bars are in standard deviation, best results of three separate experiments over three days, 3 replicates each

B) Michaelis-Menten kinetics, extrapolated from A) Km = 188 μM

In order to determine if hsp90 or a contaminating ATPase produced the ATPase activity observed in this protein prep as well as identify a control inhibitor, the protein prep was treated with the selective hsp90 inhibitor 17-AAG (31). The first test wells containing protein were treated with inhibitor and the control mix containing ATP was added immediately thereafter (Figure 16 A). The second test wells containing protein were pre-incubated with inhibitor for 30 minutes and then the working mix was added (Figure 16 B). In both experiments, no inhibition of hsp90 activity by 17-AAG was detected.

A

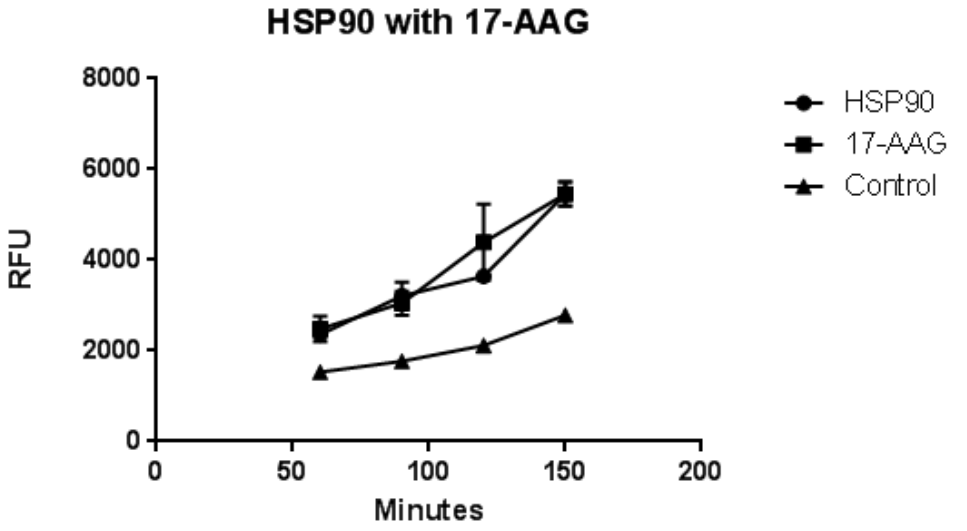

B

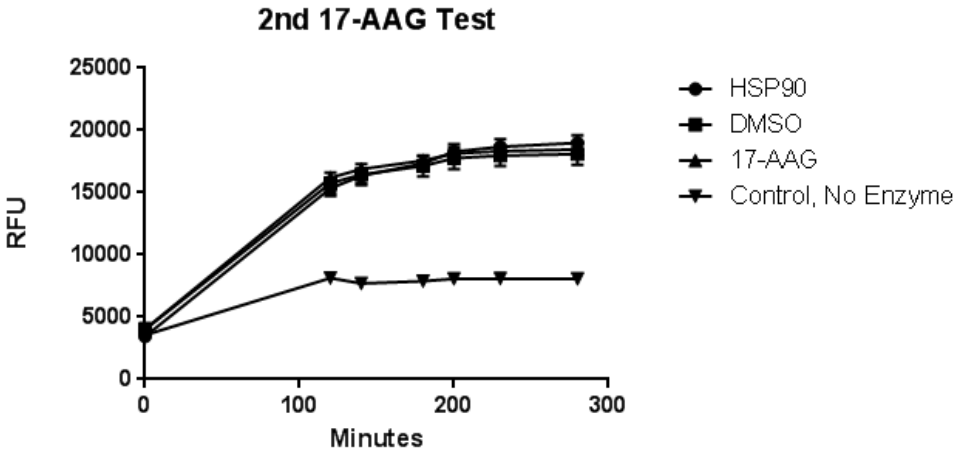

FIGURE 16: Hsp90 Prep Treated With 17-AAG
Best results of three separate experiments over three separate days

A) 6.25µg protein treated with 20µM 17-AAG with 500µM ATP added immediately. Control is no protein added with only inhibitor and working mix containing ATP.
B) 6.25µg protein pre-incubated with 20µM 17-AAG for 30 minutes before 500µM ATP added. Control is no protein added with only inhibitor and working mix containing ATP Error bars are in standard deviation. Three replicates.

Recombinant kinesin heavy chain motor domain was optimized in the PiPer assay in the same order as for hsp90. The first optimization step was the enzyme titration in which the optimal amount of protein was determined to be 700ng per well and the assay run time was determined to be 160 minutes because the optimal protein amount was still linear at this point

(Figure 17). The R^2 for concentrations 0.0875µg to 0.7µg per well were 0.98 in a linear regression fit. Conversely, a linear fit for concentrations 0.0875µg to 1.400µg produces a R^2 value of 0.94 using a linear regression curve fit. This means that the signal starts to saturate after 0.7µg.

A

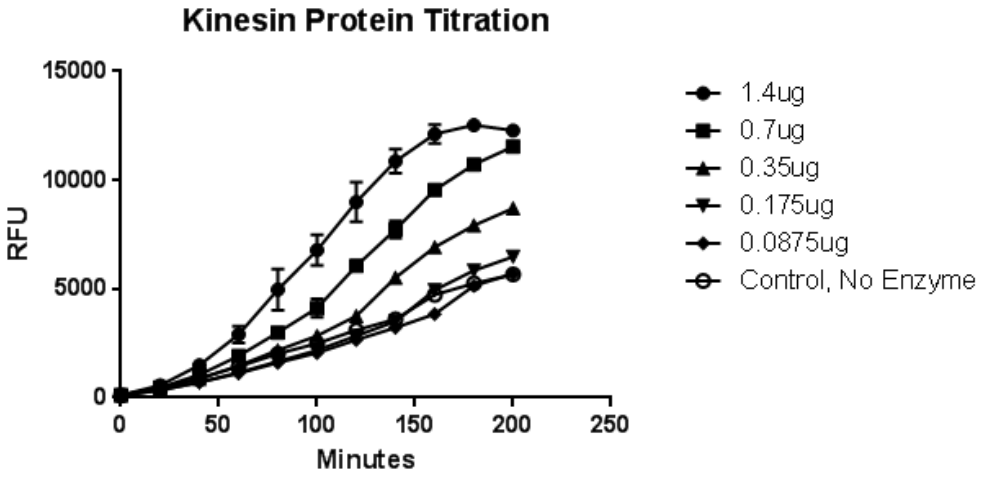

B

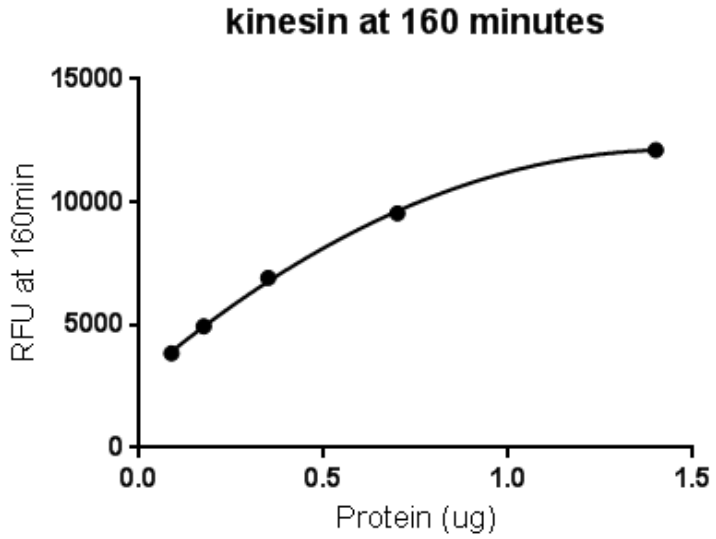

FIGURE 17: Enzyme Titration Kinesin Heavy Chain Motor Domain
Best results of three separate experiments over three separate days

A) Enzyme titration of kinesin heavy chain motor domain over time in minutes Error bars are in standard deviation. N = 3
B) RFU vs protein amount (ug) at 160 minutes.

Each test well in the substrate (ATP) titration was loaded with 0.7μg as determined by the enzyme titration. Kinesin was treated with six concentrations of ATP and 500μM ATP was chosen to be the substrate concentration because 500μM ATP produced sufficient signal compared to background(Figure 18A). Based on the Michaelis-Menten kinetics, the Km was estimated to be 53.85μM, which is similar to the published Km of 79± 8 (Figure 18 B) (46).

A

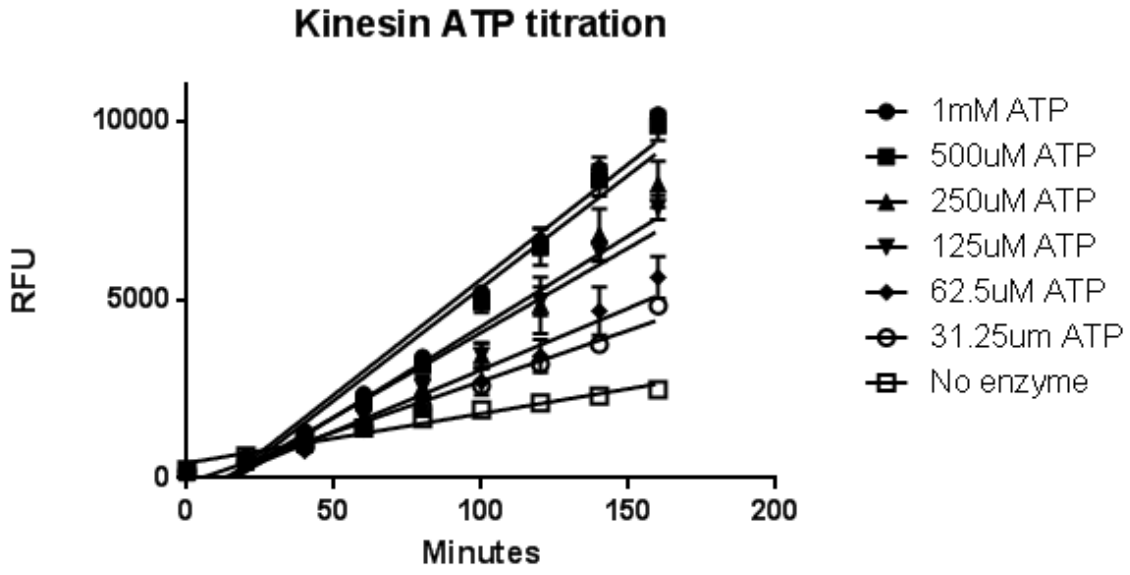

B

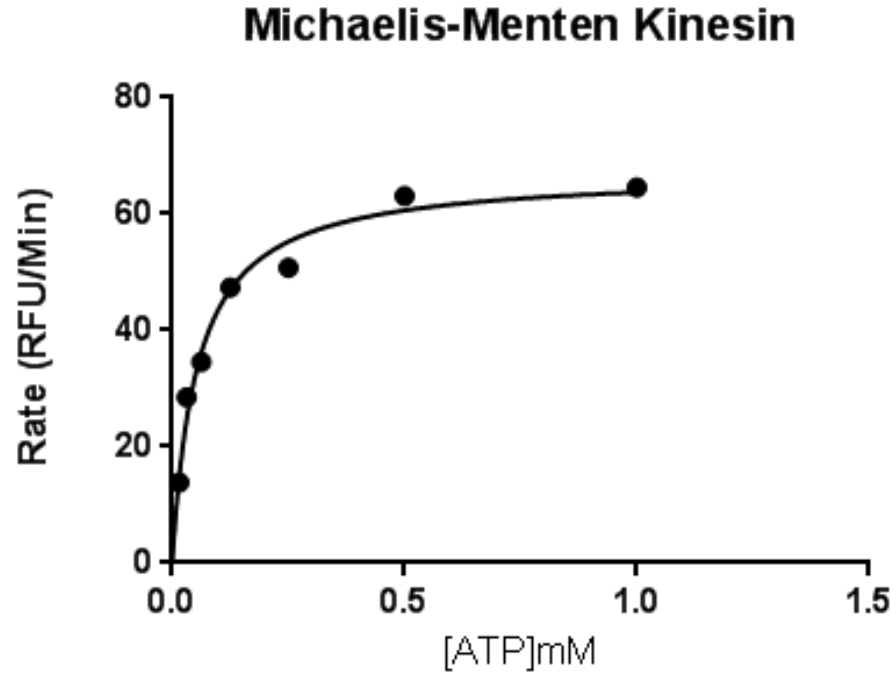

FIGURE 18: Substrate Titration Kinesin Heavy Chain Motor Domain
Best results of three separate experiment over three separate days

A) Relative fluorescence units over time in minutes for six concentrations of ATP. Error bars are in standard deviation, N = 3
B) Michaelis-Menten kinetics, extrapolated from A)

To date there are no known selective small-molecule inhibitors of this kinesin heavy chain motor domain so the recommended control inhibitor is AMP-PNP, a non-hydrolyzable analog of ATP. Kinesin was not inhibited by AMP-PNP, however it appears to have increased its activity (Figure 19).

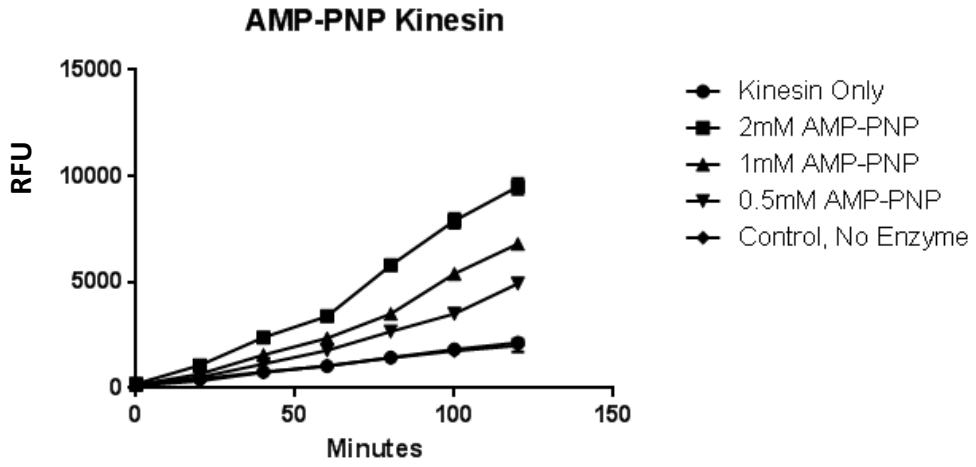

FIGURE 19: Kinesin Treated With AMP-PNP
Controls are kinesin and working mix containing ATP for the positive control and working mix and buffer only for the negative control.
Error bars are in standard deviation. N= 3
Best results of three separate experiments over three separate days

The final enzyme that was optimized in the PiPer assay was myosin. The unique thing about myosin compared to kinesin and hsp90 is that with those two enzymes did not require a special buffer, whereas myosin required a buffer that is high in salt concentration (Figure 20). Kinesin and hsp90 are active in a Tris only buffer, whereas myosin requires a high salt concentration for activity. Using the high salt buffer, the enzyme titration of myosin determined that 50μg/mL of protein would give a sufficient signal while minimalizing the amount of enzyme required per experiment (Figure 21).

A

B

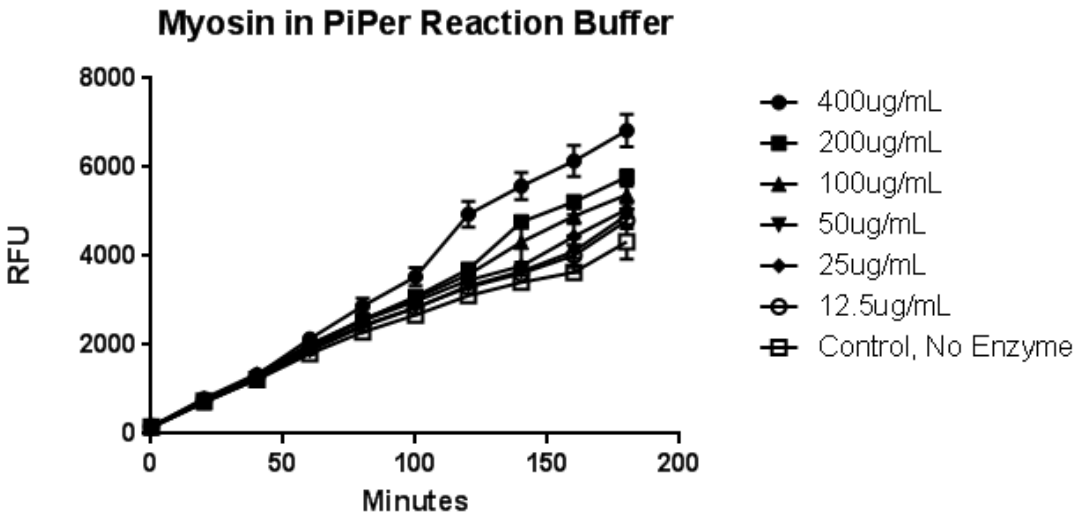
Myosin in PiPer Reaction Buffer
RFU
8000
6000
4000
2000
0
0
50
100
150
200
Minutes
400ug/mL
200ug/mL
100ug/mL
50ug/mL
25ug/mL
12.5ug/mL
Control, No Enzyme

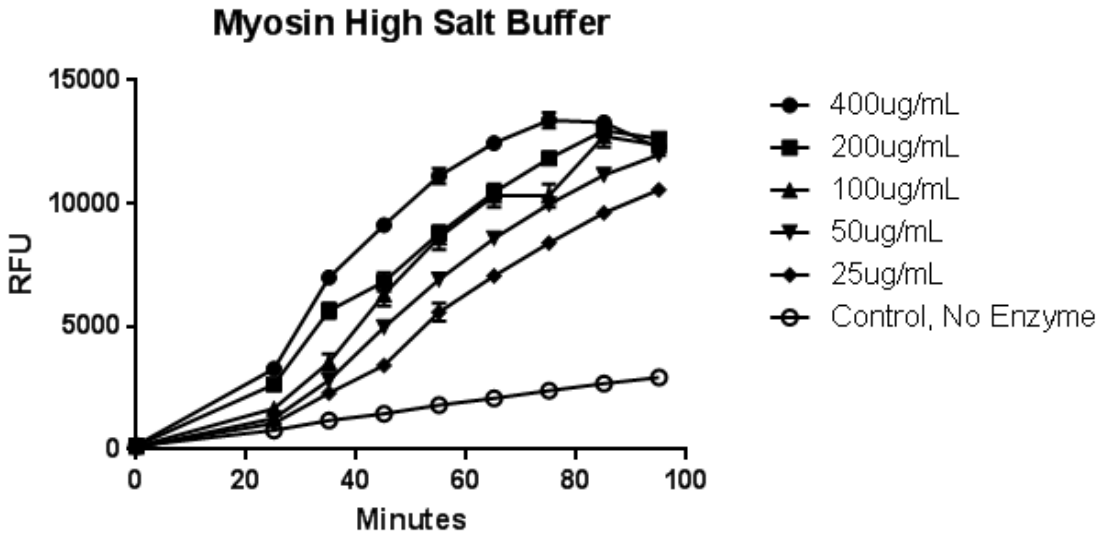

FIGURE 20: Myosin Enzyme Titration Testing Reaction Buffers
Best results of three separate experiments over three separate days

A) Myosin in PiPer reaction buffer (100mM Tris-HCl, pH 7.5)
B) Myosin in high salt buffer (50 mM Tris-HCl, pH7.9, containing 0.23 M KCl, 2.5 mM CaCl2). Error bars represent standard deviation N = 3

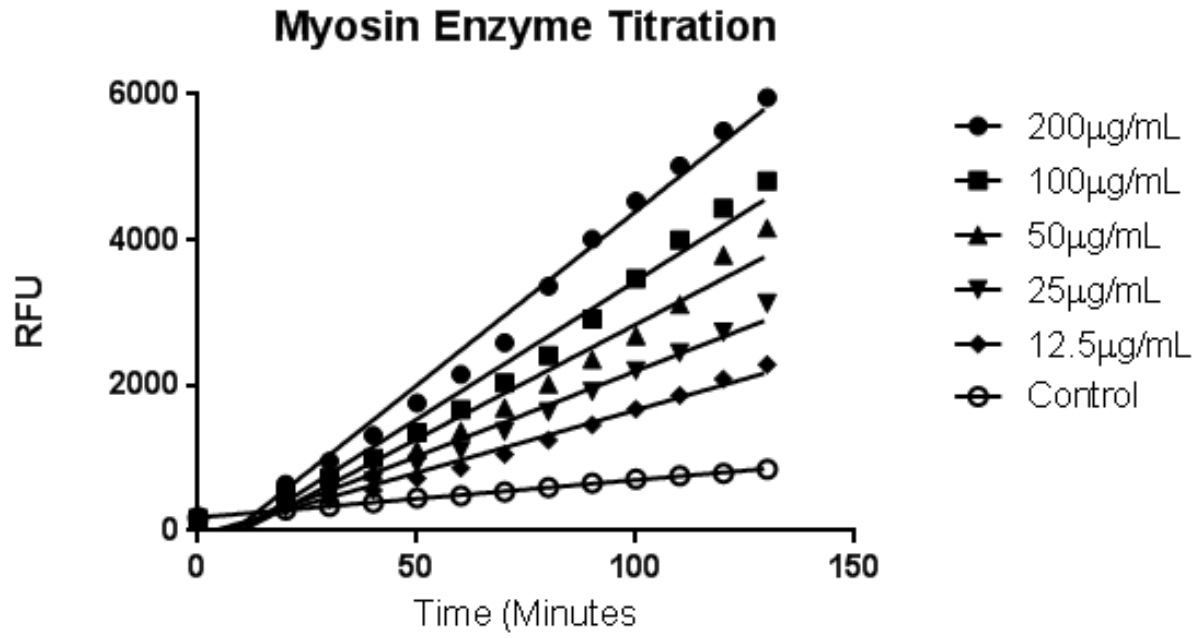

FIGURE 21: Myosin Enzyme Titration in PiPer Assay.
Enzyme titration of myosin over time in minutes.

Best results of three separate experiments over three different days
Error bars in standard deviation, N = 3

The results from the substrate titration found that 0.25mM ATP is an optimal substrate concentration for myosin in the PiPer assay (Figure 22 A). The Km calculated by the Michaelis –Menten curve was 189μM (Figure 20 B); which is consistent with the publish Km of 130 ± 40 (47).

A

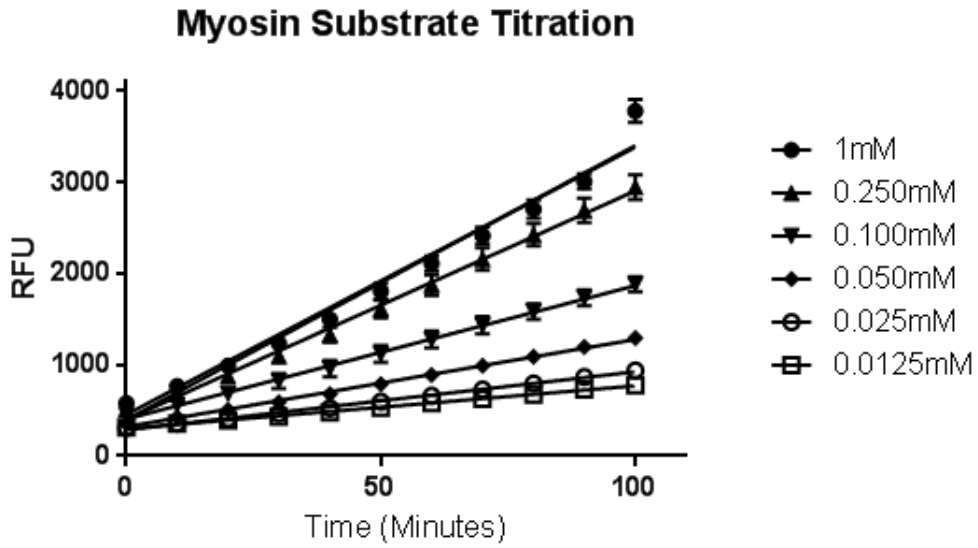

B

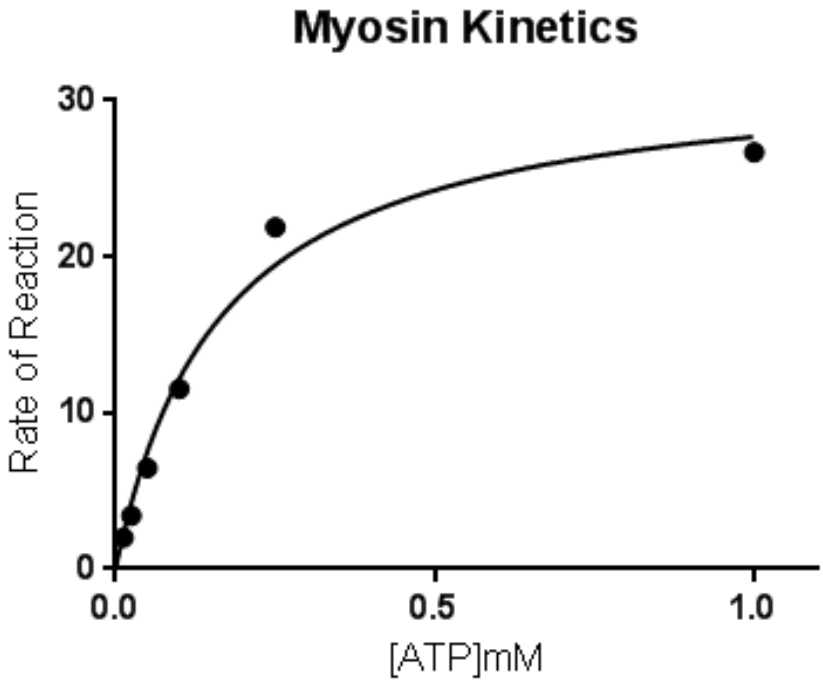

FIGURE 22: Myosin Substrate Titration
Best results of three experiments over three separate days

A) Relative fluorescence units over time in minutes for six concentrations of ATP. Error bars are in standard deviation, N = 3
B) Michaelis-Menten kinetics, extrapolated from A)

4.5 DISCUSSION

In order to show that a compound is selective for hsp90, the compounds should be tested against other ATPases. To accomplish this myosin and kinesin were chosen. Before each enzyme is tested against the hit compounds they first had to be optimized in the PiPer assay. The goal of the optimization was to identify the minimal amount of protein that produced a strong single, the minimal amount of substrate that is required to get a strong signal, and validate that the assay could detect a control inhibitor for each enzyme. For the hsp90 prep the enzyme and substrate titrations produced clear and reproducible results. However, the Km value that was determined by the substrate titration was 188.3μM and the published Km for yeast hsp90 is 300μM (47). Also 17-AAG failed to inhibit the ATPase activity of this protein prep. 17-AAG is a well-known hsp90 inhibitor and should have inhibited the ATPase activity of this protein prep. Given these two results there must be a contaminating ATPase in the protein prep even though the SDS-PAGE appears to show relatively pure yeast hsp90 (Figure 13). In the future, the hsp90 prep could be further cleaned up with a size exclusion column (49).

In the kinesin optimization, the amount of enzyme required in the assay was consistent with the published findings (46). However, when kinesin was treated with AMP-PNP there was actually an increase in activity compared to the control. There are a few possibilities as to why this happened. One possibility is that the AMP-PNP is dirty with inorganic phosphate. If that is the case then the AMP-PNP can be cleaned up with a phosphate column. The other possibility is that the AMP-PNP is dirty with ATP. This can also be cleaned up with a column. The final possibility is that AMP-PNP could be increasing the activity of one of the enzymes in the enzyme-coupled assay (50).

The enzyme and substrate titrations of myosin produced reliable and reproducible results. The Km calculated by the Michaelis-Menten curve was 189μM, which is consistent with the published Km of 130 ± 40 (50). The next step for myosin is to identify a control inhibitor. N-benzyl-p-toluene sulphonamide (BTS) was one suggestion to use as a control inhibitor, but it inhibits myosin interactions with f-actin and may not be useful for this study. As mentioned in the introduction in chapter 1, purealin inhibits cytoplasmic dynein and myosin exclusively, so it may be a good choice. Another option is to use AMP-PNP if it can be cleaned up.

5.0 FUTURE DIRECTION

The continuation of this study will need to first focus on completing the optimization of the three enzymes in the PiPer assay. This will include either further purifying hsp90 or purchasing pure enzyme. 17-AAG should have inhibited the hsp90 prep but did not (45). Once the compounds are tested in the PiPer assays and if they are shown to be selective for hsp90 ATPase activity they will need to be further validated against GR ligand binding. Compounds that do not inhibit any of the ATPases including hsp90 may be GR antagonists. In order to test the compounds for GR antagonism compounds should be tested in a GR ligand binding assay such as a fluorescence polarization (FP) assay (52, 10). The FP assay will include a GR ligand attached to fluorescent tracer compound. When the labeled GR-ligand binds GR, the FP signal is increased and when a test compound interferes with this binding FP will be decreased. A compound's ability to antagonize GR could be further explored with a GR-Reporter assay. The reporter assay includes a GR response element that is attached to a gene coding for luciferase (52). When an activated GR bound to GR agonist comes in contact with the response element the luciferase will be expressed and luciferase signal will be high. If a compound is a GR

antagonist it will prevent GR activation and there will be little or no luciferase activity. The ultimate conclusion result of these studies is might be the discovery of a novel selective hsp90 inhibitor that does not inhibit kinesin or myosin and does not block GR binding and activation. A secondary possibility of a positive result for these studies might be the discovery of a novel selective inhibitor of the GR.

References

1.) Cancer Facts and Figures 2015. American Cancer Society. http://cancer/research/cancerfactsstatistics/cancerfactsfigures2015/index
2.) Kapitein, L.C., et al., Probing intracellular motor protein activity using an inducible cargo trafficking assay. Biophys J, 2010, **99**(7): p. 2143-52
3.) Höök, P. and R.B. Vallee, The dynein family at a glance. J Cell Sci, 2006.\, **119**(Pt 21): p. 4369-71.
4.) Gohta Goshima and Ronald D. Vale. 2003. The roles of microtubule-based motor proteins in mitosis: comprehensive RNAi analysis in the Drosophila S2 cell line. JCB 162: 1003-1013
5.) Firestone AJ et al. 2012. Small-molecule inhibitors of the AAA+ ATPase motor cytoplasmic dynein. Nature. **484**(7392):125-9
6.) Giuliano KA, DeBiasio RL, Dunlay RT, et al. High-Content Screening: A new approach to easing key bottlenecks in the drug discovery process. J Biomol Screen. 1997;2:249–259.
7.) William Buchser et al. Assay Development Guidelines for Image-Based High Content Screening, High Content Analysis and High Content Imaging. Assay Guidance Manual [Internet]. 2012
8.) Hager G et al. 1999. Using Inducible Vectors to Study Intacellular Trafficking of GFP-Tagged Steroid/Nuclear Receptors in Living Cells. Methods **19**: 386-39
9.) Johnston PA et al. 2012. Development and Validation of a High-Content Screening Assay to Identify Inhibitors of Cytoplasmic Dynein-Mediated Transport of Glucocorticiod Receptor to the Nucleus. Assay and Drug Devel Tech **10:** 432-56
10.) Daghestani HN et al. 2012. Characterization of inhibitors of glucocorticoid receptor nuclear translocation: a model of cytoplasmic dynein-mediated cargo transport. Assay Drug Dev Technol. **10**(1):46-60. doi: 10.1089/adt.2010.0367
11.) Robinson-Rechavi et al. 2003. The Nuclear Receptor Superfamily. J Cell Sci. **116**: 585-586.
12.) Heitzer, M. D., I. M. Wolf, E. R. Sanchez, S. F. Witchel, and D. B. DeFranco. 2007. Glucocorticoid receptor physiology. Rev. Endocr. Metab. Disord.**8**:321–330.
13.) Galigniana, M. D., J. M. Harrell, P. R. Housley, C. Patterson, S. K. Fisher, and W. B. Pratt. 2004. Retrograde transport of the glucocorticoid receptor in neurites requires dynamic assembly of complexes with the protein chaperone hsp90 and is linked to the CHIP component of the machinery for proteasomal degradation. Brain Res. Mol. Brain Res. **123**:27–36.

14.) Pratt, W. B., M. D. Galigniana, Y. Morishima, and P. J. Murphy. 2004. Role of molecular chaperones in steroid receptor action. Essays Biochem.**40**:41–58
15.) Pearl LH, Prodromou C. 2000. Structure and in vivo function of Hsp90. Curr Opin Struct Biol **10**(1):46–51
16.) Jhaveri K, Taldone T et al (2012) Advances in the clinical development of heat shock protein 90 (Hsp90) inhibitors in cancers. Biochim Biophys Acta 1823:742–755
17.) Kamal A, Thao L et al (2003) A high-affinity conformation of Hsp90 confers tumour selectivity on Hsp90 inhibitors. Nature 425(6956):407–410
18.) Vallee, R.B., et al., Dynein: An ancient motor protein involved in multiple modes of transport. J Neurobiol, 2004, **58**(2): p. 189-200
19.) Kardon, J.R. and R.D. Vale, Regulators of the cytoplasmic dynein motor. Nat Rev Mol Cell Biol, 2009, **10**(12): p. 854-65
20.) Gleave, E.S., et al. A structural analysis of the AAA+ domains in Saccharomyces cerevisiae cytoplasmicdynein .J.Struct.Biol.(2014)
21.) Melkonian, K.A., et al., Mechanism of dynamitin-mediated disruption of dynactin. J Biol Chem, 2007, **282**(27): p. 19355-64
22.) Schroer, T., Dynactin. Annual review of cell and developmental biology, 2004, **20**(1): p. 759.
23.) Yeh TY et al. 2012. Dynactin's pointed end complex is a cargo-targeting module. Mol Biol Cell.**23**: 3827-3837

24.) Nation Center for Biotechnology Information. PubChem Substance Database, http://pubchem.ncbi.nlm.nih.gov (assessed February 12, 2015)
25.) https://www.cbligand.org/PAINS/retrieve_struct1.php?dir=wrk86669&showtype=bad
26.) Instant Jchem 6.1.3, 2014 ChemAxon (http://www.chemaxon.com)
27.) SYBYL 8.0, Tripos International, 1699 South Hanley Rd., St. Louis, Missouri, 63144, USA
28.) Kull FJ et al. 1996. Crystal structure of the kinesin motor domain reveals a structural similarity to myosin. Nature. 1996 Apr 11;380(6574):550-5.
29.) Fang, Y. I.; Yota, E.; Mabuchi, I.; Nakamura, H.; Ohizumi, Y. 1997. Purealin blocks the sliding movement of sea urchin flagellar axonemes by selective inhibition of half the ATPase activity of axonemal dyneins. *Biochemistry* 36 (50): 15561-7.
30.) Hartson SD, Matts RL. 2012. Approaches for defining the Hsp90-dependent proteome. Biophys Biochim Acta **1823**:656–667
31.) McClellan AJ, Xia Y et al. 2007. Diverse cellular functions of the Hsp90 molecular chaperone uncovered using systems approaches. Cell **131**(1):121–135
32.) Jackson S. 2013. Molecular Chaperones. Topics in Current Chemistry **328:**155-240
33.) Jakob U, Scheibel T et al. 1996. Assessment of the ATP binding properties of Hsp90. J Biol Chem **271**(17):10035–1004
34.) Panaretou B, Prodromou C et al. 1998. ATP binding and hydrolysis are essential to the function of the Hsp90 molecular chaperone in vivo. EMBO J **17**(16):4829–4836
35.) McLaughlin SH, Ventouras LA et al. 2004. Independent ATPase activity of Hsp90 subunits creates a flexible assembly platform. J Mol Biol **344**(3):813–826
36.) Tsutsumi S, Mollapour M et al. 2012. Charged linker sequence modulates eukaryotic heat shock protein 90 (Hsp90) chaperone activity. Proc Natl Acad Sci USA **109**:2937–2942

37.) Kerns EH and Di L (2008) Drug-like Properties: Concepts, Structure Design and Methods. Elsevier Text Book
38.) Lipinski CA et al .1997. Experimental and Computational Approaches to Estimate Solubility and Permeability in Drug Discovery and Development Settings. Advanced Drug Delivery Reviews. **23**: 3-25
39.) Congreve M et al. 2003. A "Rule of 3" for Fragment-based Lead Discovery?. Drug Discovery Today. **8**: 876-877
40.) Veber DF et al. 2002. Molecular Properties that Influence the Oral Bioavailability of Drug Candidates. J Med Chem. **45**: 2615-2623
41.) Muegge I .2003. Selection Criteria for Drug-Like Compounds. Med Res Rev. **23**: 302-321
42.) Goodsell DS. The RCSB PDB "Molecule of the Month". http://dx.doi.org/10.2210/rcsb_pdb/mom_2008_12
43.) PiPer Assay Manual
44.) Youker et al. 2004. Distinct Roles for the Hsp40 and Hsp90 Molecular Chaperones during Cystic Fibrosis Transmembrane Conductance Regulator Degradation in Yeast. Mol Biol Cell. 15: 4787-4797
45.) Availa C, Kornilayev B, and Blagg B. 2006. Development and optimization of a useful assay for determining Hsp90's inherent ATPase activity. Bioorganic & Medicinal Chemistry **14**: 1134-1142
46.) Böhm K J et al. 2000. Effect of temperature on kinesin-driven microtubule gliding and kinesin ATPase activity. FEBS Letters. **466**: 59-62
47.) Murphy CT, Rock RS, Spudic JA. 2001. A myosin II mutation uncouples ATPase activity from motility and shortens step size. Nature Cell Biol. **3**: 311- 315
48.) Richter K et al. 2008. Conserved Conformational Changes in the ATPase Cycle of Human Hsp90. J Biol Chem. **283**(26): 17757-17765
49.) Jakob U et al. 1995.Structural Organization of Procaryotic and Eucaryotic Hsp90. J Biol Chem. **270**: 14412-14419
50.) Motojima F and Yoshida M. 2003. Discrimination of ATP, ADP, and AMPPNP by Chaperonin Gro EL. J Biol Chem. **279**(29): 26648-26654
51.) Murphy CT, Rock RS, Spudic JA. 2001. A myosin II mutation uncouples ATPase activity from motility and shortens step size. Nature Cell Biol. **3**: 311- 315
52.) Lin S et al. 2002. A high-throughput fluorescent polarization assay for nuclear receptor binding utilizing crude receptor extract. Anal Biochem. **300**(1):15-21
53.) Zhai Y et al. 2007. Activation of Pregnane X Receptor Disrupts Glucocorticoid and Mineralocorticoid Homeostasis. Molecular Endocrinology. **21**(1):138-147

.